The DØ Upgrade
Central Fiber Tracker

Technical Design Report

Table of Contents

Chapter I. - Overview……..…….…..2

Chapter II. - Description of Mechanical Structure……..…….…….14

Chapter III. - Scintillating and Clear Fiber……18

Chapter IV - VLPC's, Cassettes and Cryosystem……..……29

Chapter V - Readout Electronics…….……36

Chapter VI - System Test…….……..42

Chapter VII - Fabrication and Assembly …….…….….46

Chapter VIII - Monitoring and Calibration……..68

[Title and Table of Contents pages reconstructed from hardcopy; TOC page numbers adjusted for this version. SG, 29-August-1999]

Chapter I. Overview

I.l Introduction

The DØ detector identifies, over a wide pseudorapidity region, electrons, muons, quarks and gluons materialized as jets, and neutrinos inferred from missing transverse energy. This is achieved with fine grained, hermetic electromagnetic and hadronic liquid argon calorimetery, muon detection using thick magnetized iron, and non-magnetic inner tracking.

Up to now, the DØ detector has collected a total integral luminosity of about 100 pb^{-1}. The collaboration has used these data to do a great deal of physics, including the discovery of the top quark.

Currently our collaboration is engaged in the upgrade of the DØ detector. The upgraded detector will operate after the construction of the Main Injector, at which time the Fermilab Tevatron luminosity will reach $2*10^{32}$ /cm^2/sec. Also, the time interval between beam bunches will decrease from the present 3.5 μs to 396 ns, and eventually to 132 ns sometime during Run II.

The detector changes which will occur in the DØ upgrade are driven both by the technological challenges of operating at the Main Injector and in order to take full advantage of the physics opportunities which will be available with the higher luminosities of Run II.

The central fiber tracker discussed in this report is a part of the upgrade of the DØ tracker. In addition to the new tracking system, the DØ upgrade includes the following components: a 2 Tesla superconducting solenoid magnet, preshower detectors in the central and forward regions, a new muon system, new calorimeter electronics, and improvements to the trigger and DAQ systems.

I.2 Performance criteria for physics goals - tracking and triggering

We review briefly the general requirements of the tracker necessary for the DØ physics goals. Many of the topics raised here can be found in DØ Notes [1], [2], [3], [4],and the Tev_2000 Study [5].

I.2.1 Top quark physics

In the Tevatron the main source of t quarks is the production of top quark pairs. Each top quark decays into a Wb pair , and the W boson subsequently decays into a charged lepton plus neutrino, or into two jets. Thus it is valuable to have a tracker capable of tagging$b$ quarks. This tagging is accomplished by measuring the impact parameters of the decay products of B particles. The scale of the precision of the measurement of the impact parameter is set by a typical vertex distance of 300 μm and the tracking system has to be capable of reconstructing of particles inside the jets. The magnetic field also plays an important role in b quark tagging, for it enables one to eliminate low-momentum tracks which seem to originate from secondary vertices because of multiple scattering. The magnetic field also helps to calibrate the calorimeter energy scale, and enhances electron identification by making it possible to compare the momentum of an electron with the energy it deposits in the calorimeter (E/p).

I.2.2 Electroweak physics

The fundamental quantity of Electroweak Physics is the mass of the W boson. In the Standard Model the W mass is related to the Z boson mass by the relation $M_W = M_Z*\cos\theta_W$. This relation is modified by radiative corrections resulting from the loop diagrams containing t and b quarks and the Higgs boson. Thus precise measurements of M_W and M_{top} test Standard Model and constrain the Higgs mass. DØ measures the$W$ mass based on the electron decay [6]: $W \rightarrow e + \nu$. The error on the W mass due to the present tracker's poor determination of the vertex and electron position is 37 MeV; the new tracker should reduce this error to near zero. The error on the$W$ mass from the uncertainty of the electron energy should also decrease because the E/P ratio will provide an additional tool for the calibration of the calorimeter. In addition, the new tracker's momentum resolution should be good enough to enable us to measure M_W in the muon channel (the resolution of the detectors in the muon system is too poor for a measurement of W mass).

I.2.3 New phenomena

Signatures of physics beyond the Standard Model will also be looked for in Run II. Various avenues will be explored, one of which is the supersymmetric

extension of the Standard Model (SUSY). SUSY predicts the existence of many new particles which are the partners of the Standard Model particles, one or more of which may be discoverable at DØ during Run II. The signatures of the supersymmetric particles are multiple, low energy leptons (compared to W decay leptons) and missing transverse energy. (The decays of SUSY particles lead in the final state to the lightest supersymmetric particle (LSP), which is stable and does not interact in the detector causing missing transverse energy)

To search for supersymmetric particles and other new particles or new physics beyond the Standard Model, the detector needs to have an excellent missing transverse energy resolution, large coverage in rapidity, good vertexing and good low energy lepton triggering and identification. The role of the tracker in the measurement of the transverse energy is to provide good vertexing in a multiple interaction environment.

The tagging of b quarks will also make it possible to look for a light Higgs boson, which in the Standard Model decays to b quark pairs 82% of the time.

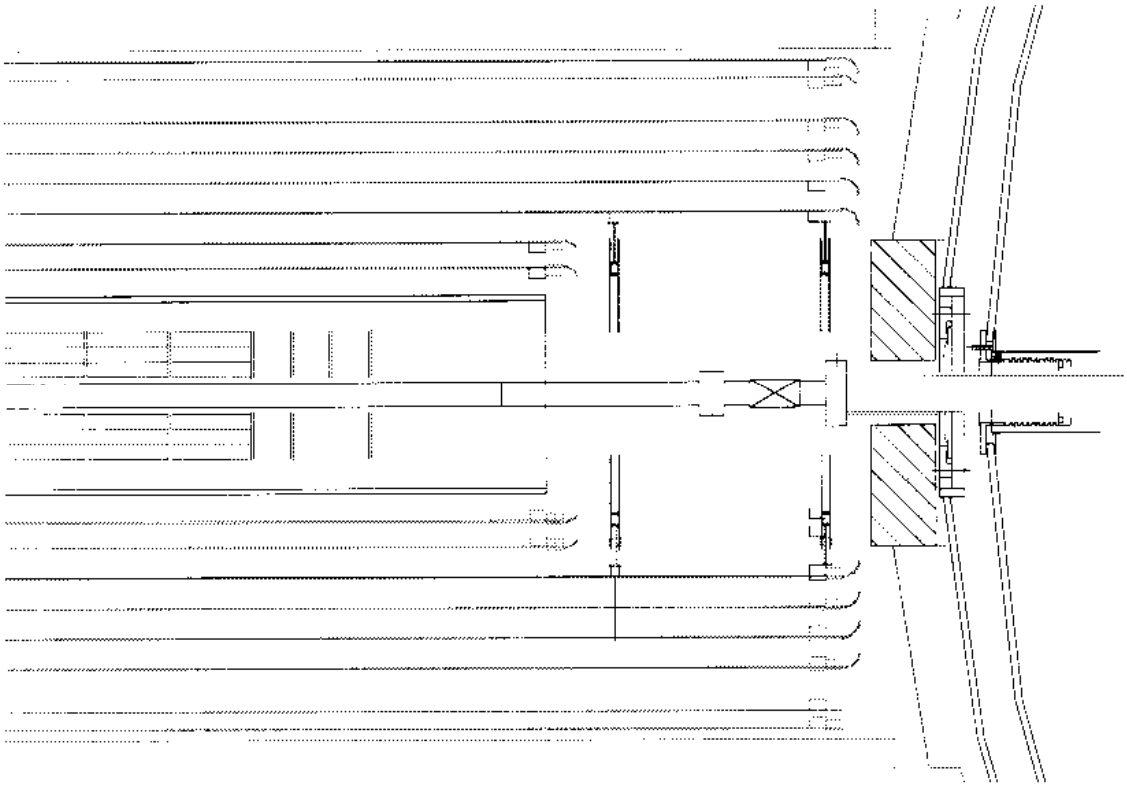

Figure I-1 Schematic View of the DØ upgrade tracking system

I.3 Overall design concept

A schematic view of the Central Fiber Tracker (CFT) is shown in Fig. I-1. The baseline design of the CFT calls for scintillating fibers completely covering 8 concentric support cylinders occupying the radial space from 20 to 50 cm. The detector will contain approximately 77,000 fibers. A fiber doublet layer oriented with the fibers in the axial direction (i.e. parallel to the beam line) will be mounted on each of the eight support cylinders. An additional doublet layer oriented in either the *u* or *v* stereo angle of approximately 2^o will be mounted on successive cylinders, so that from the smallest radius outward the orientations on the cylinders will be *xu-xv-xu-xv-xu-xv-xu-xv* . The diameter of the scintillating fibers will be 835 microns (775 micron active diameter) and the lengths of the fibers will range from 166 to 252 cm. Each scintillating fiber will be mated, through an optical connector, to a clear fiber waveguide which will pipe the scintillation light to a Visible Light Photon Counter (VLPC). The clear fiber waveguides will vary in length between approximately 8 to 11 meters. Additional details of the tracker design are given in Table I-1 below.

Layer	Radius cm	# of Fibers per sector	# of Fibers per layer	# of Fiber Ribbons	Fiber pitch in microns	Active length (m)
A	19.99	16	1280	10.0	979.3	1.66
AU	20.15	16	1280	10.0	987.2	1.66
B	24.90	20	1600	12.5	975.8	1.66
BV	25.60	20	1600	12.5	982.1	1.66
C	29.80	24	1920	15.0	973.4	2.52
CU	29.97	24	1920	15.0	978.6	2.52
D	34.71	28	2240	17.5	971.7	2.52
DV	34.87	28	2240	17.5	976.2	2.52
E	39.62	32	2560	20.0	970.4	2.52
EU	39.78	32	2560	20.0	974.4	2.52
F	44.53	36	2880	22.5	969.5	2.52
FV	44.69	36	2880	22.5	972.9	2.52
G	49.43	40	3200	25.0	968.7	2.52
GU	49.59	40	3200	25.0	971.8	2.52
H	51.43	44	3520	27.5	916.1	2.52
HV	51.59	44	3520	27.5	919.0	2.52

Table I-1 Design parameters of the Central Fiber Tracker

The small (835 micron) fiber diameter gives the fiber tracker an inherent doublet layer resolution on the order of 100 microns, which combined with the silicon in the axial view will give DØ good momentum resolution for charged particles. In order to preserve this resolution capability, the location of the individual fibers must be known to an accuracy better than 50 microns in the r-phi direction. This will be achieved by building up accurate ribbons of fibers and placing them precisely onto the support cylinders. Doublet layer resolution of 90 microns has been achieved with cosmic rays in a test of a large-scale fiber tracker prototype [I-3]. Details of this test are given in Section VI. The other significant factor in the momentum resolution of the upgrade tracking system is the amount of material contributing to multiple scattering of charged particles. The effect of material on both momentum and mass resolution is discussed in the following section. To minimize this effect, care must be taken in the mechanical design of the support cylinders to keep the material budget as small as possible while at the same time preserving the rigidity and roundness of the cylinders required for the accurate positioning of the scintillating fibers. More details of the mechanical tolerances and structure are given in sections II and VII.

The small fiber diameter (and large channel count) also gives the tracker sufficient granularity both to find tracks and to trigger in the complex event environments expected in Run II. A high doublet layer efficiency is essential to the fiber tracker performance, and studies have shown that to maintain this efficiency the mean number of detected photoelectrons per fiber must exceed 2.5 for a minimum ionizing particle. This number is a function of the intrinsic photoyield of the scintillator, the light transmission properties of the fiber and connectors, and the quantum efficiency of the VLPC. In the aforementioned cosmic ray test, a mean of about nine photoelectrons per fiber was obtained, leading to doublet layer efficiencies of better than 99.5%. To guarantee good efficiency in the final detector, the roughly 75,000 channels of VLPCs delivered from the manufacturer (Boeing North American) must have less than 0.1% dead channels and each channel must satisfy a series of performance requirements, including quantum efficiency, gain and noise count.

Only the fibers themselves will be susceptible to any radiation damage. Studies indicate that no more than a 30% reduction in light yield is expected for the innermost fiber cylinder, with correspondingly less damage to fibers at larger radii.

I.3.1 Momentum resolution

The expected transverse momentum resolution for the DØ upgrade tracking system is shown in Figure I-2. The calculation of the resolution was done with the following parameters: the resolution of the scintillating fiber doublet is 100 microns (based on the results of the cosmic ray test [7]), the resolution of the silicon barrels is 10 microns, the non-active material in the silicon detectors has a radial distribution as given in Figure 1.7 of the DØ Silicon Tracker Design Report [8], the thickness of the barrels supporting the scintillating fibers is 0.086 g/cm^2 for barrels 3 and 4 and 0.065 g/cm^2 for all other barrels [9], and the interaction vertex is known with a precision of 35 microns.

The transverse momentum resolution at pseudurapidity $\eta=0$ may be parametrized as: $\sigma p_T/p_T=\sqrt{0.015^2 + (0.0014\cdot p_T)^2}$. This is better than the resolution for the precise configuration assumed in [10]; based on that paper the W mass resolution from $W \to \mu\nu$ decays should be less than 25 % worse than that from $W \to e\nu$ decays.

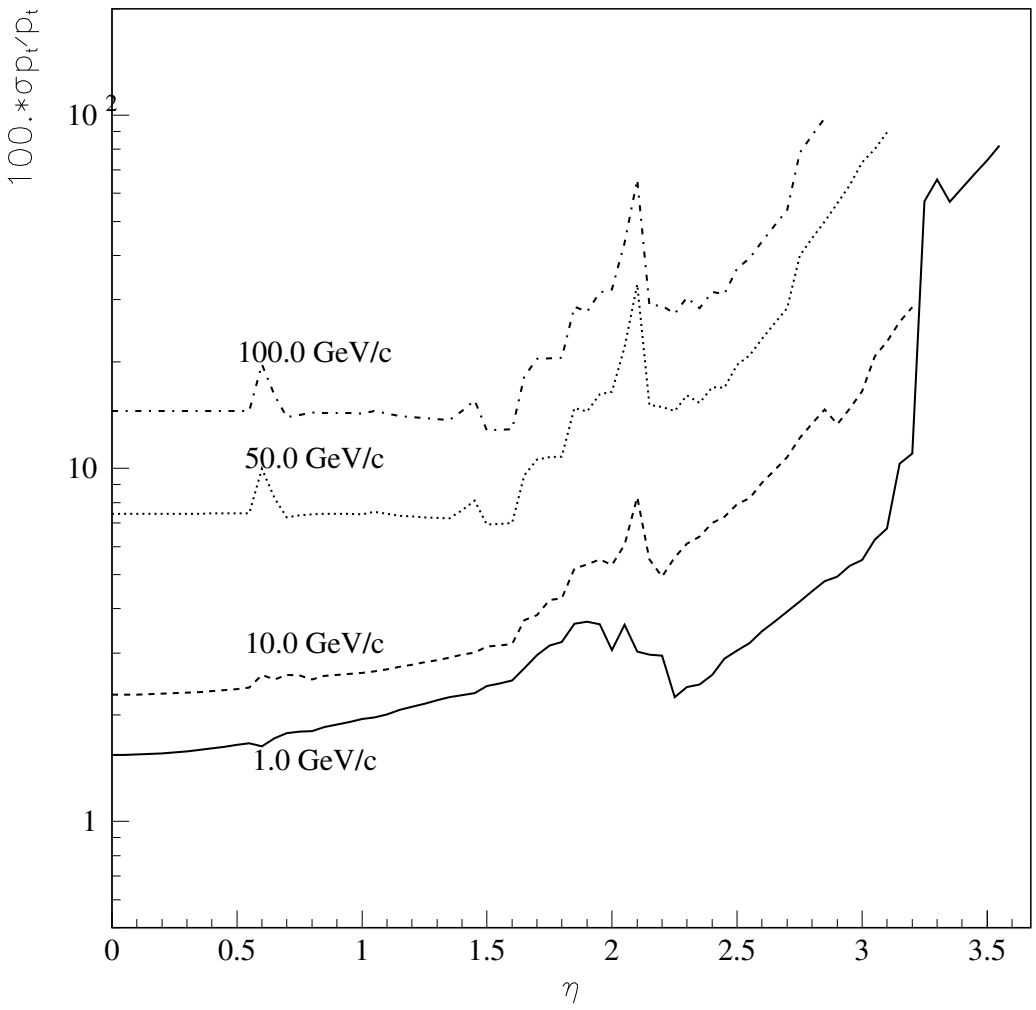

Figure I-2 Resolution as a function of η assuming 35 μm vertex resolution.

The effect of the thickness of the cylinders supporting the scintillating fibers is shown in Figure I-3. The resolution, in %, at η=0, is shown as a as a function of the supporting cylinder for: a 1 GeV/c track in Fig. I-3a), for a 40 GeV/c track in Fig. I-3b), and for the mass of the J/Ψ particle from $B \rightarrow J/\Psi$ events in Fig. I-3c). The thickness of the fiber tracker support cylinders has no impact on the momentum resolution of 40 GeV/c tracks, which are characteristic of $W \rightarrow l\ \nu$ decays. Conversely, the resolution of the mass of the J/Ψ peak worsens from 34 MeV/c^2 to 50 MeV/c^2 when the cylinder thickness increases from 0.05 g/cm^2 to 0.2 g/cm^2. The J/Ψ mass peak will be used to establish the

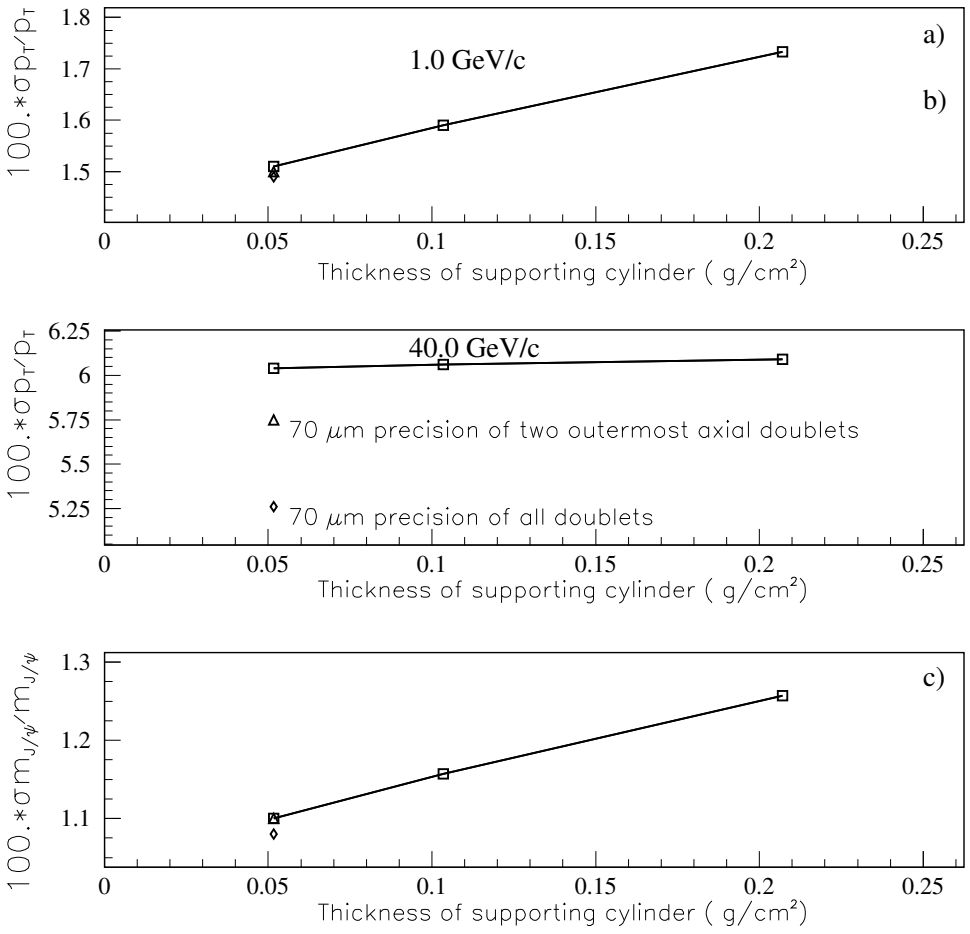

Figure I-3 Resolution, in %, as a function of thickness of supporting cylinder at η=0: a) for a track with momentum of 1 GeV/c, b) for a track with momentum of 40 GeV/c, and c) for the mass of the J/ψ particle from B→J/ψ events.

momentum scale of the DØ detector and that is one of the reasons why we are trying to construct the thinnest cylinders possible. The error of the momentum scale also has an impact on the determination of the energy scale of the calorimeter when the quantity E/p is used. The error of the momentum (energy) scale contributes to the systematic error of the W mass determined from $W \to \mu\nu$ ($W \to e\nu$) decays [10].

In Figure I-3 we also show how the momentum and mass resolution would change if the resolution of the scintillating fiber doublets were improved to 70 microns, either in the two outermost axial doublets or in all doublets (which could be achived with

smaller diameter fibers).The resolution of low momentum tracks and of the J/Ψ mass peak remain unchanged, while the momentum resolution of 40 GeV/c tracks improves from 6.04 % to 5.75 % to 5.26 %, respectively. This improvement was judged insufficient to justify the increased cost and complication involved in the building of a tracker with scintillating fiber doublets of 70 micron resolution.

I.3.2 Impact parameter resolution

The expected resolution of impact parameter is shown in Figure I-4. The solid line shows the resolution of the combined silicon and scintillating fiber tracker while the dashed line shows the resolution of the silicon detector only. The scintillating fiber tracker contributes
significantly to the quality of the measurement of the impact parameter.

To evaluate the effect of *b* tagging on the identification of top quark events we have generated a Monte Carlo sample of top quark production events (with m_{top} = 160 GeV) using ISAJET. In addition a background sample of *W* and four or more jets was generated using VECBOS and ISAJET for parton fragmentation. These events were then simulated and reconstructed. A tagging scheme that requires at least three tracks reconstructed each with impact parameter significance (the ratio of impact parameter to its error) greater than
three retains more than 50% of top events and only 2% of background events.

I.3.3 Triggering

The central fiber tracker is an important element of the DØ trigger system. Due to the fiber tracker's fast response time, the total time of the collection of signals from the central fiber tracker from one interaction is considerably shorter than the 132 ns bunch spacing expected in Run II. This enables the fiber tracker to participate in the DØ Level 1 trigger without contributing any dead time.

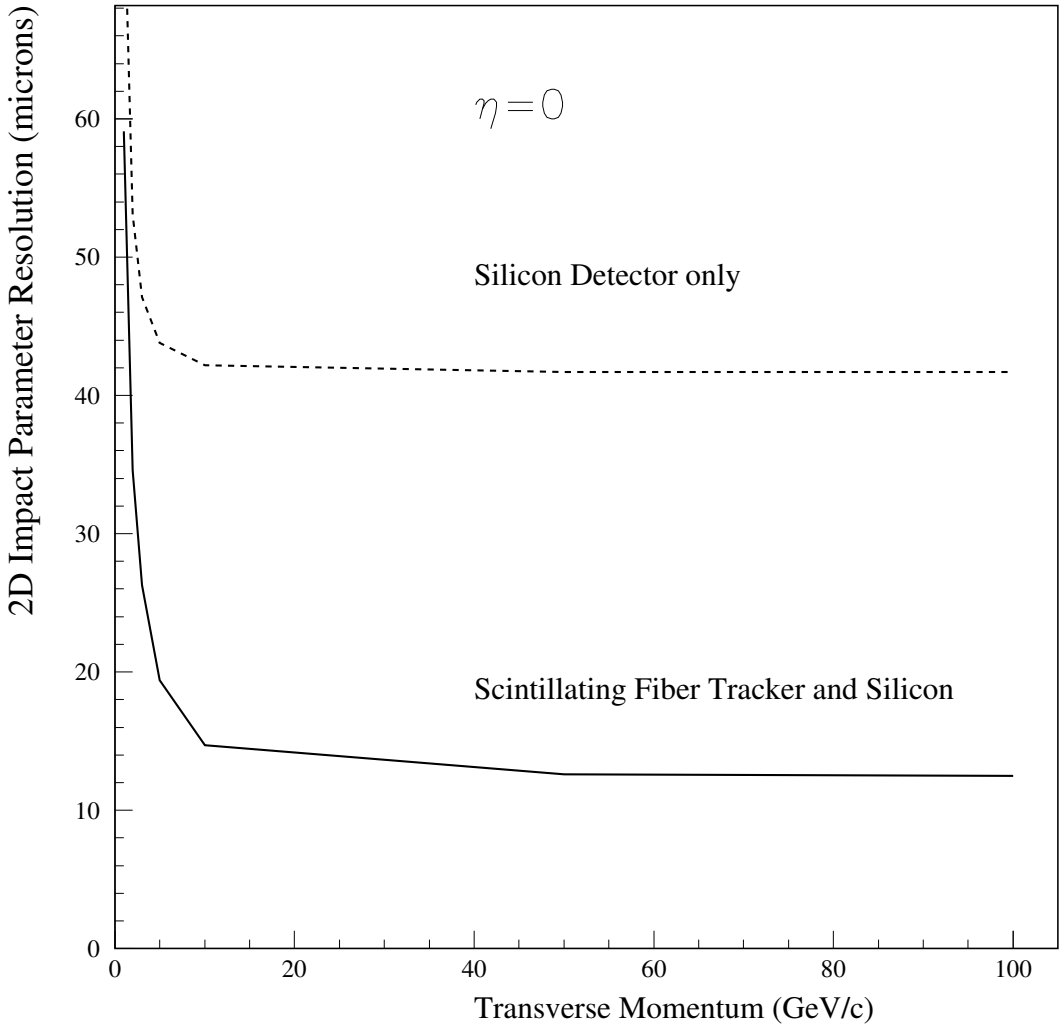

Figure I-4 2-dimensional impact parameter resolution a η=0 vs transverse momentum

The trigger is implemented using field programmable gate arrays, FPGA's. First, the signals from singlet axial layers are combined into hits. Coincidences between eight hits form tracks. The tracks are combined with central preshower clusters to form an electron trigger, and with muon detectors to form a muon trigger. However, in order to perform this operation in the 4 μs time allowed for Level 1 processing, the tracker has to be divided into 80 equal azimuthal sectors for parallel processing.

A high p_T (p_T > 10 GeV/c), efficient lepton trigger is necessary to accumulate large samples of top quarks , and *W* and *Z* bosons. However, for other physics channels there is also the need for a low p_T lepton trigger.

The momentum scale of the tracking system will be established by reconstructing the J/Ψ mass from the decay of $J/\Psi \rightarrow \mu\mu$; these muons have a momentum of about 1.5 GeV/c. Large samples of J/Ψ are needed to study the tracking system's uniformity and time variation. The precision of the momentum scale also impacts the precision of the determination of the energy scale of the calorimeter from the E/P ratio.

A low p_T lepton trigger is also needed for the detection of *b* jets, which often contain low p_T leptons. Identification of *b* jets is an important tool in top quark identification and Higgs searches.An efficient, low p_T lepton trigger will improve our sensitivity in the search of new particles. For example, the production of supersymmetric objects such as winos and zinos lead to final states with multiple leptons. Although these quaginos are predicted to be quite massive, after their decays the final state leptons are often at low p_T.

The CFT trigger adds some constraints to the mechanical design of the fiber tracker, particularly in the placement of the scintillating fibers. For the offline tracking one could conceivably correct for the misalignment of fibers with the use of position constants, but that is not possible for the online trigger. This means that it is not sufficient to simply know the location of the axial fibers accurately. The fibers must be placed precisely upon their support cylinders such that any skew away from parallel to the beam axis is limited to within 40 μm from end to end. The routing of the clear waveguide fibers bringing the scintillation light to the photodetectors is also complicated by the 80 sector trigger geometry of the CFT.

I.4 References

[1] "The DØ Upgrade",S. Abachi et al., Fermilab-Conf-**95/177-E.**

[2] "DØβ", DØ Note **1733** (1993).

[3] "Magnetic Tracking", DØ Note **1993** (1993).

[4] "B Tagging and Electron Identification", DØ Note **2054** (1994).

[5] "Future Electro-weak Physics at the Fermilab Tevatron". Report of the Tev_2000 Study Group, Fermilab-Pub-**96/082**, edited by D. Amidei and R. Brock (1996).

[6] "DØ Results on W Boson Properties", submitted to HEP97, Jerusalem, Israel (1997)

[7] B. Baumbaugh et al, IEEE Trans. on Nucl. Sci **43** (1996), 1146.

[8] "DØ Silicon Tracker Design Report", DØ Note **2169** (1994).

[9} K. Krempetz, private communication.

[10] "Effect of Muon Momentum Resolution on W Mass Measurement with the Upgrade

DØ Detector, DØ Note **2687** (1995)

Chapter II. Description of Mechanical Structure

II.1 Introduction

The Central Fiber Tracker will combine with the silicon microstrip detector to provide the charged particle tracking for the DØ detector in Run II. The CFT will also provide a track trigger, and will combine with other detectors to form first-level electron and muon triggers. The requirement that the CFT deliver efficient tracking and triggering with high resolution directly impacts on the mechanical structure of the fiber tracker. Each of the approximately 78,000 scintillating fibers must be placed accurately onto their respective support cylinders, and their positions must remain stable over the duration of the experiment. This implies a very strong and rigid support system. However, it is also important to make the support cylinders as thin as possible to minimize effects of multiple scattering. The effects of cylinder thickness on momentum and mass resolution were shown in Fig. I-3 in the previous section. For a track traversing the detector at normal incidence to the cylinders, the total thickness of the active fiber ribbons is 0.05 radiation lengths. The goal for the mechanical support structure is to keep the additional contribution from the support cylinders below 0.04 radiation lengths (0.17 g/cm^2).

The general layout of the fiber tracker was introduced in subsection I.3. In this section the mechanical tolerances are discussed for the key elements making up the detector. The fabrication and assembly of these elements is given in more detail in Section VII.

II.2 Tolerances

The cylindrical geometry of the tracker makes it useful to express fiber coordinates and position errors in the coordinate system consisting of **z**, the linear coordinate running along the beam axis, **R**, the radius, and the azimuth $\mathbf{\Phi}$ or the circumferential coordinate $\mathbf{R} \times \mathbf{\Phi}$.

Tests done with a 3000 channel prototype of the fiber tracker indicate that a hit resolution of ~ 80 μm perpendicular to the principal fiber axis is attainable. This sets the precision required for overall fiber placement in the detector: the goal is to built a detector where each fiber is at its nominal position within an uncertainty of better than 50 μm RMS in **R**-$\mathbf{\Phi}$, i.e. along the cylinder circumference, and ~ 150 μm in **R**.

In addition to this requirement given by offline track reconstruction, triggering requires the end-to-end offset of an axial fiber relative to a parallel to the beam axis to be less then 40 μm, again measured in the **R-Φ** coordinate.

The process of "mounting" a scintillating fiber in the detector can be broken down into four separate steps:

1. Alignment of individual scintillating fibers into a precise ribbon.
2. Mounting of the fiber ribbons precisely onto support cylinders.
3. Alignment of the cylinders relative to each other and to the silicon tracker within the mechanical support frame.
4. Alignment of the tracker in the detector relative to the nominal beam line axis.

As a first step one can allocate an RMS error of ~ 20 μm to each of these procedures. Looking at the task at hand in somewhat finer detail it becomes clear that most of the random error in fiber position and direction results from the the first step, the ribbon manufacture, and that after step 2) only correlated deviations are introduced, which are subject to the more stringent 40 μm off-axis constraint over the full length of the fiber tracker.

Furthermore is must be considered that while offline track reconstruction can theoretically make use of several position constants per fiber, online triggering requires a tracker built to specification, with each axial fiber at its nominal position and parallel to the average beam axis. For the trigger the fibers on different cylinders have to line up in **Φ**. This makes the fiber spacing a function of the radius of the tracking layer, and possibly leads to the introduction of up to 16 different ribbon pitches.

II.3 Ribbons

Fiber ribbons consist of 256 fibers in two layers of 128 fibers, each layer having a precise fiber spacing of between 919 and 965 μm, depending on the tracking layer radius in the detector. In the method chosen for the CFT, precisely spaced grooves with the correct fiber pitch for a given radius are machined into a long, flat piece of flexible plastic. The plastic is inserted into a rigid, curved backing with the desired radius and the scintillating fibers are laid in and glued together to form a doublet ribbon. This technique creates curved ribbons to match the curvature of each of the support cylinders while avoiding the costly step of cutting precisely-spaced grooves into a curved surface. More details of the ribbon production are given in Section VII.1.

II.4 Support Cylinders

Support cylinders have to provide a mechanically stable and precise mounting surface for the fiber ribbons, while at the same time minimizing the amount of material presented to particles traversing the tracker.

As the principal direction of the particle trajectories is along the radial coordinate, the precision requirements in this direction are not very stringent and are mainly given by the coupling between radial and circumferential fiber coordinate introduced by grouping the fibers in ribbons of finite width. As layed out in DØ note 2010, for ribbons with a width corresponding to 128 fibers (about 115 mm) the imperfection in radial position should not exceed 150 μm RMS.

The requirement for stability against deflection under load (beam sag and shape distortion) is much more stringent. Contributions to these deflections include the weight of the support cylinder itself, the weight of the fibers mounted on the cylinder, and the effects of any inner tracking layers supported by a given cylinder. The deflections must be limited in order to keep the individual fiber displacement in **R-Φ** to within 25 μm RMS , and to within an envelope of less than 40 μm total systematic displacement variation over the full length of the tracker.

A method of fabricating carbon fiber suppport cylinders with the required cylindricity, rigidity and low mass has been developed at Fermilab. Details of the fabrication procedure and results on prototype cylinders are given in section VII.3.

II.5 Connectors

Various connector concepts have been tested. The most promising as far as ease of connection and precision of fiber alignment are concerned is the v-groove connector. Fibers are held in their relative positions exactly as given by the ribbon by means of machined v-groove connectors. After glueing and embedding the fibers into the connector, the connector's front surface is diamond-machined. The mating parts are aligned by means of precision pins inserted into holes in the connecting surfaces. The current connector design is discussed further in section VII.1.4 below.

II.6 Clear Waveguide Bundles

The clear waveguide bundles typically consist of 256 undoped fibers of the same construction and diameter as the scintillating fibers. The bundles vary in length from

about 7-11 meters, depending upon location. At the detector end the clear fibers are terminated in a v-groove connector which mates to the connector on the scintillating fiber ribbon. The connectorization at the other end of the waveguide bundles is an open question. To map the 80 trigger sectors of the CFT to the correct VLPC cassettes requires segmenting the 256 fibers in a waveguide bundle into 32 separate, 8-fiber units. Details of the waveguide bundle fabrication and testing, along with a discussion of the various clear fiber routing choices, are given in section VII.4.5 below.

II.7 Cassette Connectors

Cassette top connectors are molded from polyurethane, and hold 128 fibers. Each cassette top connector has locating pins and holes for eight 16-fiber waveguide connectors. Thus the ribbon grouping of the waveguides can be mapped into the trigger wedge grouping of the cassettes and VLPC modules. Again, as in the previous section, the exact details of the cassette top connectors will depend upon the final routing scheme chosen for the clear fiber waveguides.

Chapter III. Scintillating and Clear Fiber

III.l Introduction

The DØ CFT is constructed of scintillating fibers of 830 μm diameter and 1.7 - 2.6 m axial length which are optically connected to clear fiber waveguides of identical diameter and typically 8-10 meters in length. The choices of physical dimensions are based on the simultaneous requirements of high detection efficency per fiber element (and hence near unity efficiency for fiber doublet ribbons), high spatial resolution per fiber doublet of $\sigma \leq 100$ μm, and detector construction considerations. The fibers are manufactured by Kuraray Corporation [1] and are of multiclad structure - a core surrounded by two claddings. The clear fiber is structurally and chemically identical to the scintillating fibers, but contains no fluorescent dyes. Approximately 200 km of scintillating fiber and 800 km of clear waveguide fiber comprise the CFT.

The following is a brief description of the key elements and processes involved in the detection of light from a charged particle traversing a scintillating fiber. A much more detailed discussion of scintillating fiber tracking detectors can be found in [2].

III.2 Scintillation Light Production in Fibers

To illustrate the basic principles of scintillation light production, collection, and detection as it applies to the DØ central fiber tracker, a schematic representation of a fiber element is shown in Figure III-1. Charged particles produced in a p-pbar collision that pass through the fiber volume will deposit energy by ionization, a portion of which is converted into scintillation light. A fraction of this light is optically trapped inside the fiber and travels to the opposite ends. At one end, the light encounters an aluminum mirror coating and is reflected back into the fiber. At the other end, the fiber is mated to a clear optical waveguide fiber which "pipes" the light over some distance to a VLPC photosensor situated in available space outside of the central detector.

A variety of technically demanding challenges must be met for this technique to work well as a particle detector. The scintillating dyes must produce enough light to be detected while maintaining a low level of self-absorption. Fiber-to-fiber interconnections need to have optical transmissions near unity, the clear fiber must transmit light over large distances, and the photosensor is required to have good quantum efficiency and high rate capability.

The signal from a scintillating fiber detection element, in mean number of detected photoelectrons ($< N_{PE} >$), may be estimated from the following expression (refer to Figure III-1):

$$< N_{PE} > = \int_{\Delta\lambda} [\, S(\lambda)\;\; CT(\lambda)\;\; QE(\lambda)\,]\; d\lambda \qquad (1)$$

where: $S(\lambda)$ is the differential source term, such that $\int S(\lambda)\, d\lambda$ is numerically equal to the number of scintillation photons produced in the active medium; $CT(\lambda)$ is the light collection and transfer factor; $QE(\lambda)$ is the quantum efficiency of the photosensor. The integral is taken over the spectrum of emission wavelengths, $\Delta\lambda$, of the scintillator. In the DØ case, the factors comprising $< N_{PE} >$ are slowly varying as a function of wavelength over the emission wavelength interval, and Equation (1) can be approximated by the form:

$$< N_{PE} > \;\sim\; < S > \; < CT > \; < QE > \qquad (2)$$

where all factors assume average values over the emission spectrum.

In general, the source term depends on the nature of the energy deposition, the scintillation material, the material geometry, and the path length in the material traversed by ionizing radiation:

$$< S > \;=\; < dE/dx > \; < \Delta x > \; \Delta n_\gamma / \Delta E$$

where $< dE/dx >$ is the mean energy loss per unit length at minimum ionization in the scintillation medium; $< \Delta x >$ is the average path length of a charged particle traversing the material; and $\Delta n_\gamma / \Delta E$ are the number of photons produced per unit of deposited energy.

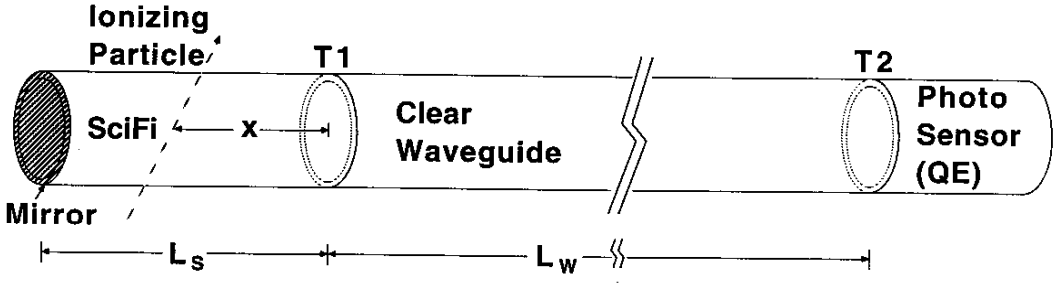

Figure III-1 Schematic of a fiber-tracking element showing a scintillating fiber of length L_S optically coupled to a clear fiber waveguide of length L_W, which transfers the light to a VLPC photosensor of quantum efficiency QE. Transmission coefficients for the optical interfaces T1 and T2 are indicated.

An ionizing particle is assumed to pass through the scintillating fiber at a distance x from the joint with the clear fiber waveguide. Light initially traveling toward the mirror is reflected back into the fiber and toward the readout end with reflection coefficient R.

The organic plastic scintillators of interest to DØ consist of several components, and hence scintillation light production in such materials is a multistep process. The polystyrene (PS) base (*~99%* by weight) absorbs energy from ionizing radiation; approximately *4.8 eV* of deposited energy is required to excite a base molecule. The relaxation time of polystyrene is slow and it is a poor intrinsic light emitter. However, the presence of the organic fluorescent dye paraterphenyl (PTP), selected for its well-matched energy level structure and at a concentration of *~1%* by weight, leads to rapid non-radiative energy transfer ($\Delta t < 1$ ns) from PS to PTP molecules via a non-radiative dipole-dipole interaction known as *Fšrster Transfer.* The PS excitations are quickly relaxed to the ground state and the excitation energy is now stored in excited PTP molecules. PTP has very high quantum efficiency (*>95%*) and rapid fluorescence decay (a few nanoseconds). The high concentration of the PTP and its short emission wavelength ($\lambda \sim 340$nm) generally limits the mean free path of such light to a few hundred microns in the plastic. To get the scintillation light out over length scales of several meters requires the incorporation of a secondary or waveshifter dye which is spectrally matched to the PTP, but which has, as an intrinsic property, minimal optical self-absorption. DØ has chosen the intramolecular proton transfer dye 3-hydroxyflavone (3HF) for this purpose. Introduced into the plastic at low concentration (1500ppm), the 3HF efficiently absorbs the 340 nm radiation from the PTP and reemits light at a much longer wavelength ($\lambda \sim 530$ nm). The choice of this emission wavelength is not arbitrary as it lies within the regime of best optical transmission in bulk polystyrene. Light at this wavelength can be successfully propagated over lengths of 4-5 meters in the scintillating fiber, and twice that distance in clear waveguide fiber. However this yellow-green light is poorly detected by conventional bialkali and multialkali photomultiplier tubes, and hence a solid-state photosensor, the visible light photon counter (or VLPC), has been selected by DØ to detect this light efficiently.

Equation (2) can provide a numerical estimate of the light yield as it applies to scintillating fibers based on the PS-PTP-3HF composition. The density of polystyrene is *1 g/cm*^{3}, and the mean energy deposition for minimum ionization is $\langle dE/dx \rangle \sim 200$ keV/mm. For a scintillating fiber element (Figure III-1), only the energy deposited in the scintillating core is relevant for light emission; the cladding materials provide for light

containment and transmission only and are otherwise inactive. For the DØ CFT, the multiclad scintillating fiber is of 830μm outer diameter, the thickness of the double-cladding wall is ~ 30μm. Hence the core diameter is d_{core} = 770 μm. Assuming the fiber is exposed to a uniform illumination of charged particles from one direction at normal incidence to the fiber axis, the average path length through the core is $\langle \Delta x \rangle = (\pi/4) \cdot d_{core}$ = 605 μm. Thus the mean deposited energy is $\langle dE/dx \rangle \langle \Delta x \rangle$ = 120 keV. The number of photons produced per unit of deposited energy is given by:

$$\Delta n_\gamma / \Delta E = (\Delta n / \Delta E)\, Q$$

where $\Delta n/\Delta E$ represents the number of excitations produced in the material per unit energy deposition (*~1 excitation/4.8eV* for polystyrene), and *Q~4%* is the quantum efficiency of the material (the fraction of the excitation that appears as fluorescence). Combining the above values, we find $\Delta n_\gamma / \Delta E$ = 1/120 photons/eV. Hence the average response of the scintillating fiber to ionizing radiation at normal incidence is $\langle S \rangle = 10^3$ photons. These photons are emitted isotropically within the scintillator and with an emission spectrum characteristic of *3HF* which is peaked near *530nm,* as Figure III-2 illustrates.

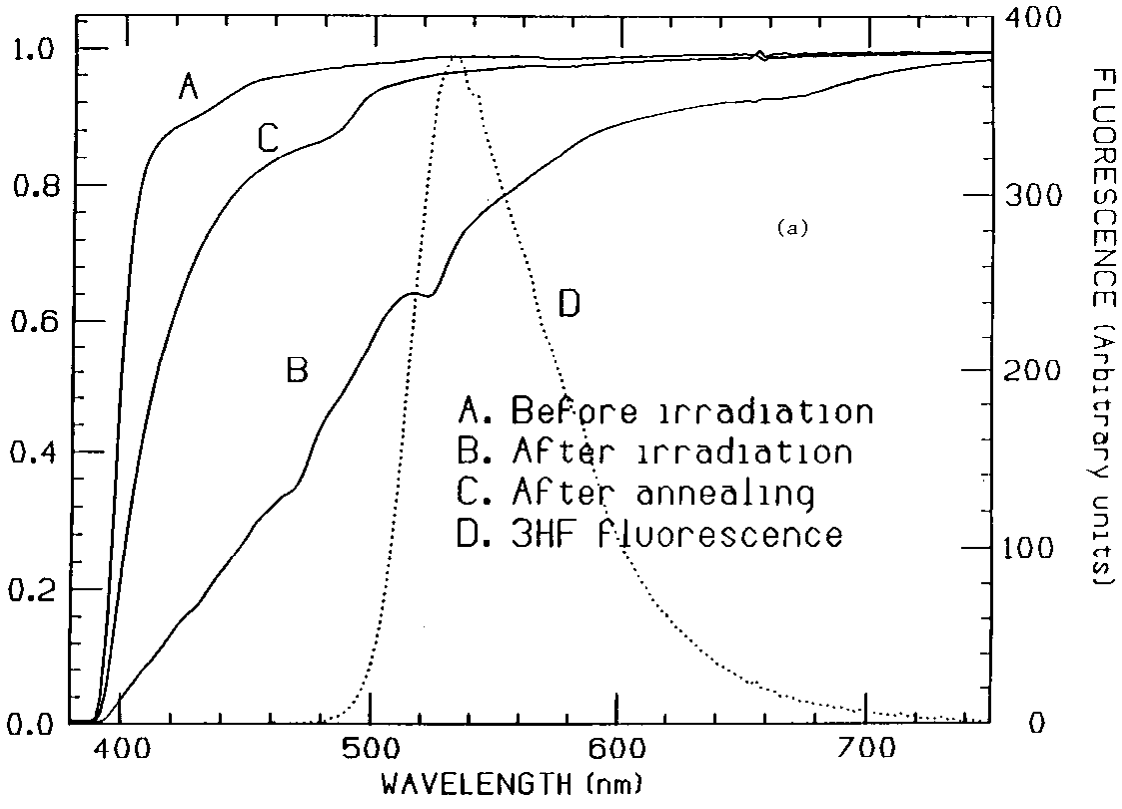

Figure III-2 Fluorescence absorption and emission of 3HF. Also shown is the optical transmission through bulk samples before and after exposure to radiation, and after annealing.

III.3 Light Collection and Transfer

Once the scintillation light has been produced, it must be collected and transferred to a VLPC photosensor. The collection and transfer factor, $\langle CT \rangle$, depends on the mechanical construction and optical properties of the scintillating fiber, waveguide fiber, optical connectors and end-mirroring of the fiber. The process consists of several steps, each of which is (in general) a function of wavelength, and may be estimated from the following expression:

$$\langle CT \rangle = (d\Omega/4\pi)\,[A_1(x)+R\cdot A_{1R}(2L_s-x)]\cdot T_1\cdot A_2(L_w)\cdot T_2$$

Here $d\Omega/4\pi$ is the effective fraction of the solid angle of scintillation light contained by total internal reflection inside the fiber in one direction; A_1 is the attenuation of the direct

scintillation light in the scintillating fiber; R is a non-zero factor only if one end of the scintillating fiber is mirrored; A_{1R} is the attenuation of the reflected component of the scintillation light in the scintillating fiber; T_1 is the transmission coefficient through the optical connector between the scintillating fiber and the waveguide fiber; A_2 is the attenuation of the scintillation light as it traverses the waveguide fiber; and T_2 is the transmission coefficient between the waveguide fiber and the photosensor. Scintillating fiber and waveguide fiber lengths are denoted by L_s and L_w respectively, and x denotes the location of the ionization site within the scintillating fiber, measured relative to the readout end.

A significant recent advance in fiber waveguide manufacture has been the development of multiclad scintillating fiber by Kuraray Corp. Surrounding a polystyrene core with the refractive index *n=1.59* are two claddings: an inner clad of polymethylmethacrylate (*PMMA*) with *n=1.49*, and an outer clad of fluoro-acrylic with *n=1.42* . The *PMMA* inner clad serves as a mechanical interface between the core and the outer clad, which are mechanically incompatible.

The multiclad fiber is both mechanically and optically superior to single-clad fiber. Assuming emission of scintillation light from a point source on the symmetry axis of a fiber with a circular cross section, the effective fraction of the light trapped by total internal reflection within the fiber in one direction is $d\Omega_{sc}/4\pi = 3.1\%$ for single-clad and $d\Omega_{mc}/4\pi = 5.3\%$ for multiclad fiber. This improvement in numerical aperture of 1.7 for multiclad fiber has been measured for scintillation light trapped and transmitted over large distances. For Kuraray multiclad "S" type fiber, typical values of the attenuation length are ~ *5 m* for the scintillating fiber and ~ *8 m* for the clear waveguide fiber. For Kuraray "Non-S" type fiber, these values are ~ 20% larger (see Figure III-3). Both of these values are superior to the corresponding performance of single-clad scintillating fiber and waveguide. Because the S type fiber is less brittle than the non-S type, this improved flexibility affords advantages in detector construction. Hence the S type is the preferred material for the fabrication of fiber ribbons for the CFT. The attenuation factors for "S" type fiber are: $A_1 = \exp(-x/5)$, $A_{1R} = \exp(-(2\,L_s - x)/5)$, and $A_2 = \exp(-L_w/8)$.

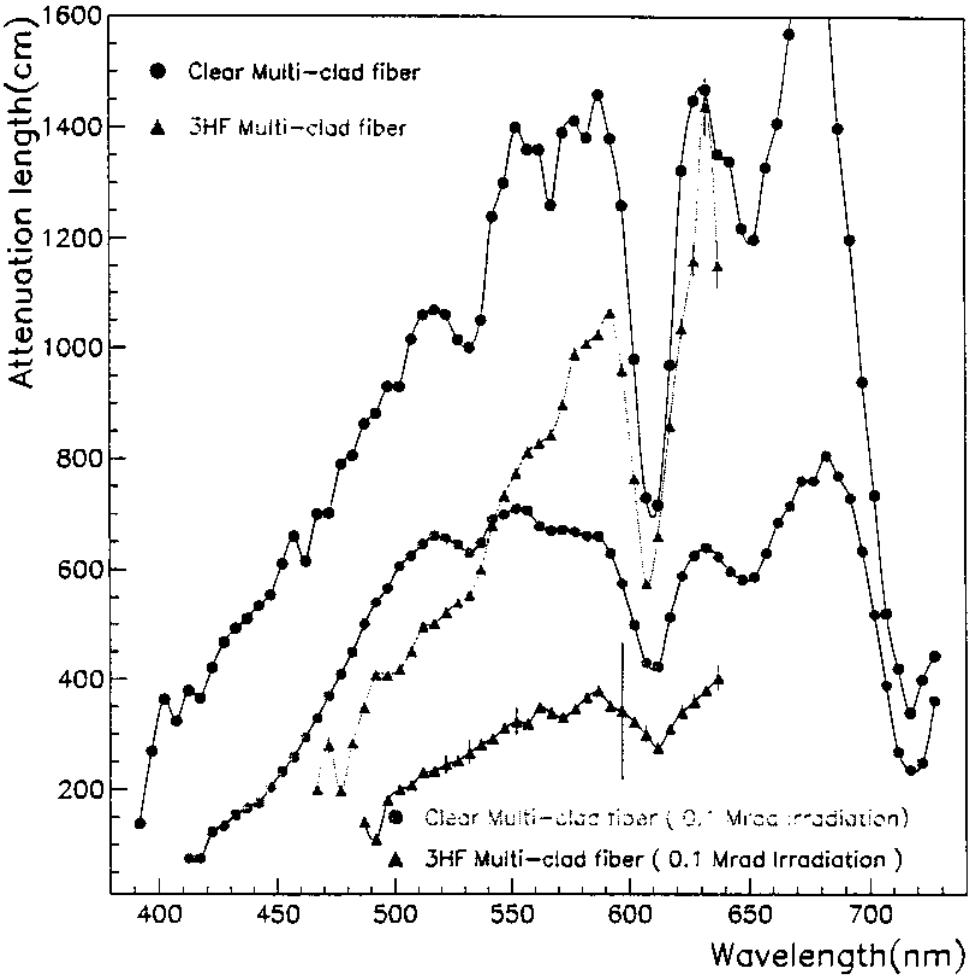

Figure III-3 Measured attenuation length as a function of wavelength for Kuraray multiclad "non-S" type scintillating and clear waveguide fiber, before and after irradiation with 100 krad of ^{60}Co.

While the light from a scintillating fiber may be viewed from either or both ends, DØ has elected to observe the light from one end only. In this case, it is desirable to mirror the "non-readout end" of the fiber, and to reflect the light that would normally escape from this end back into the fiber and hence to the photosensor. Mirroring may be applied by sputtering an aluminum coating onto the ends of the fibers, or by bringing the ends of the fibers into direct contact with a highly reflective surface such as an aluminized mylar foil. Simple foils have provided good reflectivity $R \sim 70\%$ in tests,

and the Al sputtering planned for the CFT should provide even better reflectivity (R ~ *80%*).

Transmission through optical connectors has been studied extensively. Optical transmission values of T_1, T_2 ~ 90% have been readily achieved in preliminary tests, and the expectation is that these values should be obtained routinely in large-scale systems. An important innovation in this area has been the development and use of diamond fly-cutting machines to prepare connector surfaces for optical connection. Mineral oil and Dow-Corning Q2-3067 optical couplant have been used successfully as optical coupling media.

Combining all of the above values, the average collection and transfer factor is <CT> ~ 1.5%. (see Table 1).

III.4 Total Photoelectron Yield

Table 1 summarizes the various factors that contribute to the photoelectron yield for the case of a multiclad, PS/PTP/3HF scintillating fiber 830 μm in diameter and 3 meters long, with end mirroring, optically coupled to a 830 μm diameter clear fiber waveguide 8 meters in length, and read out with a VLPC assumed to have 70% quantum efficiency. The scintillation source is assumed to originate from the midpoint of the scintillating fiber, which for the colliding beam environment would represent the worst case detected photoelectron yield. As Table 1 shows, the expected yield is $<N_{PE}>$ ~ 10 photoelectrons. This value is consistent with recent measurements in cosmic ray tests. With further refinements such as improved sputtered-aluminum end mirroring and increased VLPC quantum efficiency, a 20% increase in the detected photoelectron yield might be realized.

Figure III-4 displays the expected mean photoelectron yield per fiber as a function of η for the inner layer of the fiber tracker, assuming particles emanating from a point-source interaction at z=0. The increase in yield at high values of η is due to the increased path length for the particles in the fiber which scales with polar angle as (1/sinθ).

Term	Parameter	Parameter Value	Term Value
Source	$<S>$		10^3 *photons*
	$<dE/dx>$	*200 keV/mm*	
	$<\Delta x>$	*0.605 mm*	

	dn_γ/dE	*1/120 photons/eV*	
Collection and Transfer	$<CT>$		*1.5%*
	$\delta\Omega_{mc}/4\pi$	*0.053*	
	$A_1(x = 3m)$	*0.55*	
	$A_{1R}(2L_s\text{-}x = 3m)$	*0.55*	
	R	*0.7*	
	T_1	*0.9*	
	$A_2(L_w = 8m)$	*0.37*	
	T_2	*0.9*	
Quantum Efficiency	$<QE>$		*70%*
Mean Detected Photoelectron Yield	$<N_{PE}>$		*~10 photoelectrons*

Table 1 Parametric performance of a multiclad scintillating fiber tracking element of 830 μm diameter and 3 m length with end mirroring, optically coupled to a 925 μm diameter waveguide fiber of 8 m length, and read out with a HISTE-IV VLPCs. A scintillation point source at the far end of the scintillating fiber is assumed.

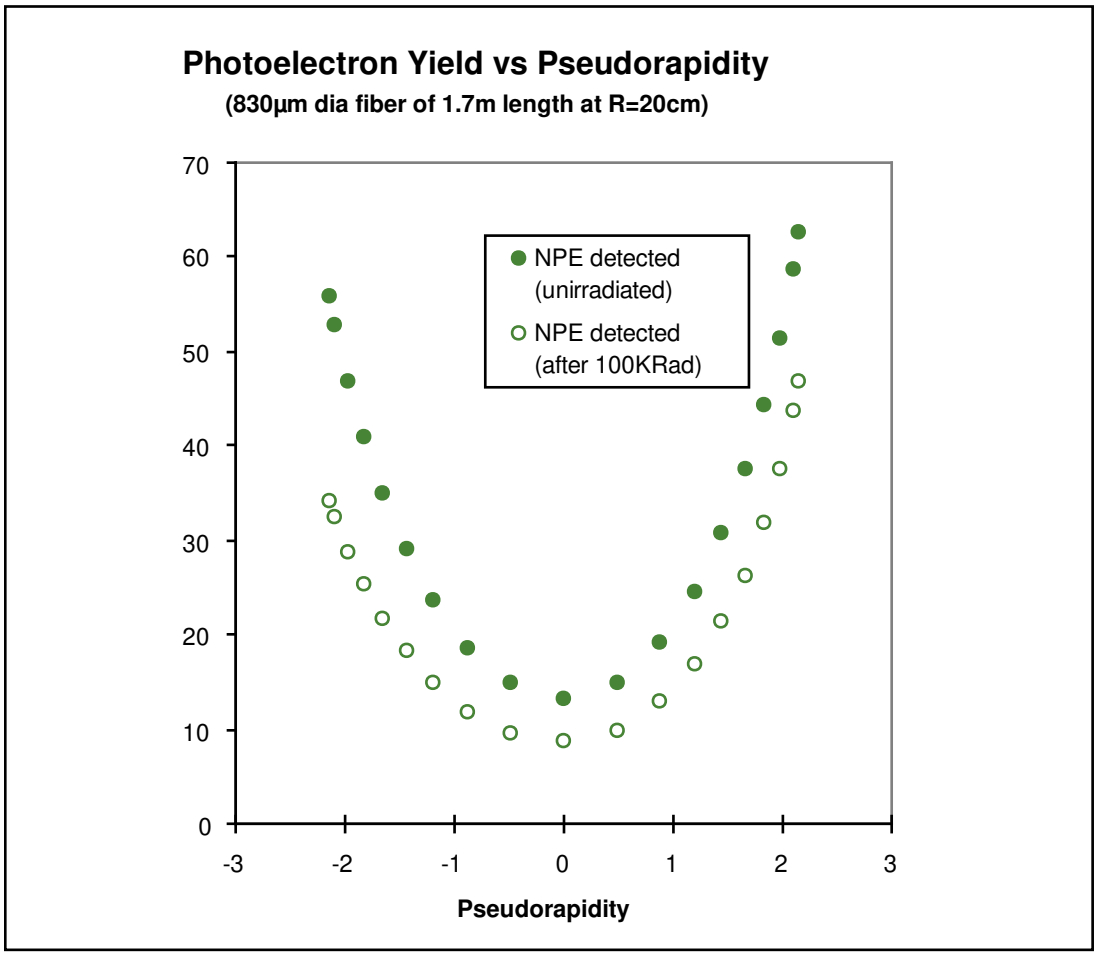

Figure III-4 Expected photoelectron yield per fiber as a function of η for the DØ CFT. The fiber length and radius correspond to the inner layer of the CFT.

III.5 Environmental Factors

Fiber performance deteriorates under integrated radiation exposures of several hundred *krads* . For luminosities expected at the Tevatron Collider and Main Injector ($L \sim 10^{32}\ cm^{-2}\ s^{-1}$), a fiber layer placed at a radius $r > 20\ cm$ from the beam should survive usefully for ~*10* years. As an additional note, it has been observed that plastic materials suffer less radiation damage if they are irradiated in an inerting atmosphere, and periodically annealed in oxygen or air between radiation exposures. Hence DØ intends to operate the CFT in an ambient atmosphere of dry N_2 gas. During shutdowns or extended periods of no beam, the detector region will be back-filled with dry air.

Polystyrene scintillators containing 3HF have been found to be photo-unstable in the presence of short wave visible light, and deterioration in the presence of sunlight, fluorescent lamps or high-intensity mercury arc flood lamps has been readily observed. However, if handled under yellow-lamps (filtered for $\lambda > 450$ nm) no deterioration is observed. Nevertheless, care must be taken to avoid any unnecessary exposure of the materials.

III.6 References

[1] Kuraray International Corporation, 200 Park Avenue, New York, NY 10166

[2] "The Use of Scintillating Fibers for Charged-Particle Tracking", R. Ruchti, Annu. Rev. Nucl. Part. Sci 1996. 46:281-319

Chapter IV - VLPC's, Cassettes and Cryosystem

IV.1 Introduction

The photodetector used in the CFT is the Visible Light Photon Counter (VLPC). It is a cryogenically operated silicon-avalanche device. The operation and development of the has been discussed extensively in the literature [1]. In this section we will give the performance specification of the production VLPC to be used in the DØ CFT and an overview of the VLPC packaging or "Cassette". Details of the VLPC cassette design can be found in the "DØ Fiber Tracker 1024 Channel VLPC Cassette Technical Design Report and Specification".[2]

IV.2 The Visible Light Photon Counter (VLPC)

The VLPC is a descendant of the Solid State Photomultiplier, an impurity band silicon avalanche photodetector.[1] It has undergone six design iterations, specified as HISTE I - HISTE VI. HISTE VI will be the version used in the DØ CFT. It is an eight element array in a 2 by 4 element geometry. Each pixel in the array has a diameter of 1 mm. A full characterization study of this device has been performed. The device performance specifications are given below: (Operation under accelerator conditions corresponding to a luminosity of $2x10^{32}$)

- Quantum Yield > 0.5
- Photoelectron threshold cut of < 2 pe for noise rate < 0.5%
- Gain > 40,000
- Operating temperature 7-10K
- Operating Bias 6-8V

This specification will guarantee a fiber-singlet hit efficiency of greater than 98%.

IV.3 VLPC Cassette

The VLPC cassette contains 1024 channels of VLPC readout and is divided into 8 modules of 128 channels each which are interchangeable and repairable. This is

illustrated in Figs. IV-1 and IV-2. Figure IV-1 shows the full cassette with readout boards attached. Figure IV-2 shows the inner components of the cassette, with the readout boards and cassette body removed. Both figures clearly show the 8-fold modularity of the cassette design.

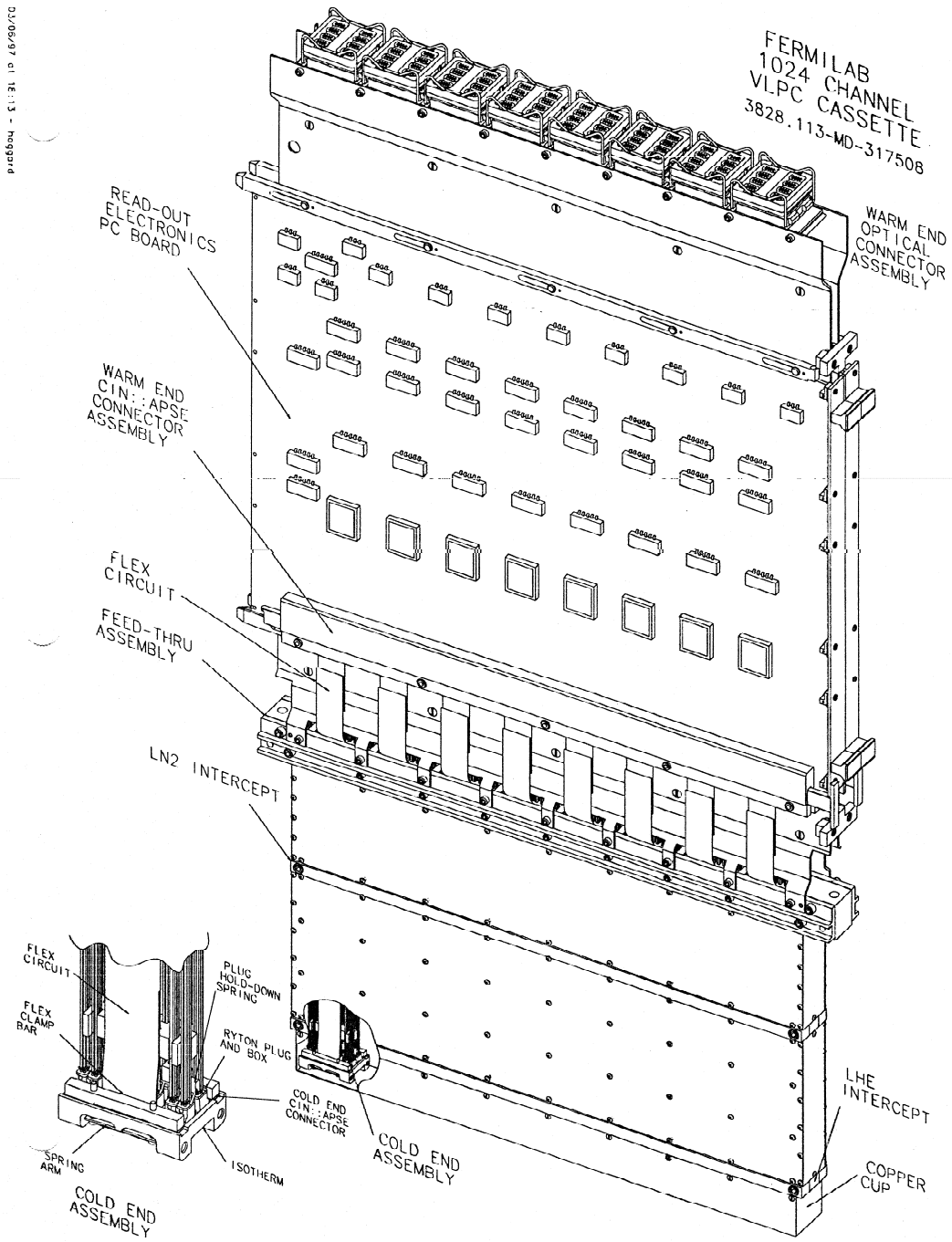

Figure IV-1 The VLPC cassette with readout electronics board attached.

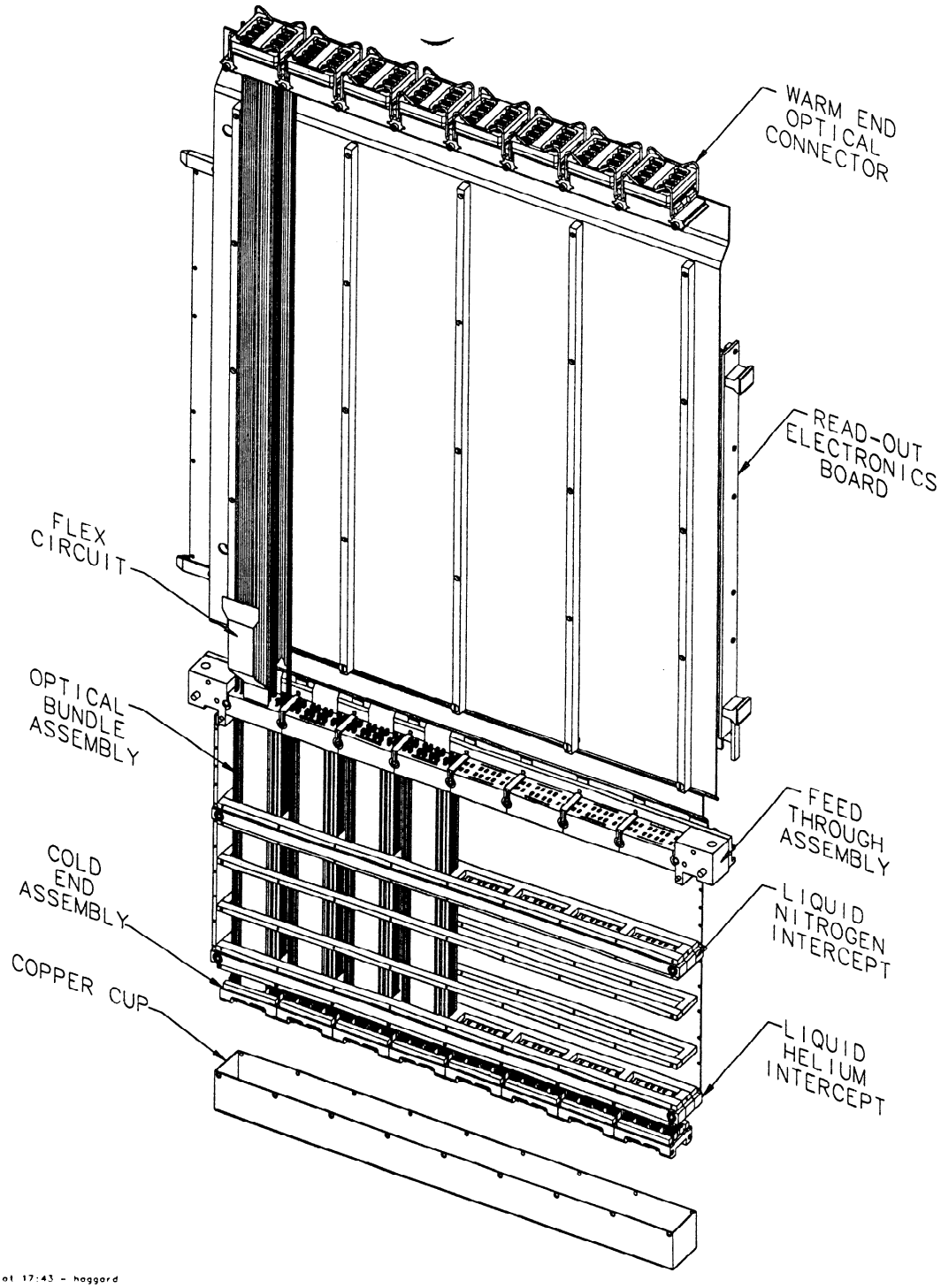

Figure IV-2 Inside view of the VLPC cassette with cassette body removed.

As stated above the HISTE VI VLPC chip will be used in the production cassettes. Sitting directly over each VLPC pixel is an optical fiber which brings the light from the detector to the VLPC chip. Each cassette module is comprised of an optical bundle assembly, a cold-end electronics assembly, and an assembly of mounted VLPC hybrids. The cold-end assembly is designed to be easily removable for repair without disturbing other modules due to the high cost and delicate nature of this device. Another important design requirement of this cassette regards the read-out electronics. Due to the nature of accelerator operations, the readout electronics boards, the PC boards which act as interface to the data acquisition system, must be removable and replaceable without removing a cassette from the cryostat. The readout electronics are discussed in detail in the following section.

The cassette, for purposes of discussion, is broken down into several major components. The cassette is distinguished as having a "cold end", that portion of the cassette which lies within the cryostat, and a "warm end", the portion of the cassette which emerges from the cryostat and is at room temperature. At the cold end, eight cold end assemblies each of 128 channels of VLPC readout are hung from the feed-through by the optical bundles and are surrounded with a copper cup at the cold end. Each cold-end assembly consists of sixteen 8 channel VLPC hybrid assemblies, the "isotherm" or base upon which they sit, the heater resistors, a temperature measurement resistor, cold end flex circuit connectors and the required springs, fasteners and hardware. A blowup of the cold-end assembly is show in Fig. IV-3. Running within the cassette body from top to bottom are eight 128 channel optical bundle assemblies which accept light from the detector wave guides connected to the warm end optical connectors at the top of the cassette and pipe the light to the VLPC's mounted at the cold end (see Fig. IV-2). The electronic read-out boards are located in rails which are mounted to the warm end structure and are connected electrically with the cold end assemblies via kapton flex circuits. In addition, the electronics boards are connected to a backplane card and backplane support structure by card edge connectors and board mount rails. The flex circuits and read-out boards are electrically and mechanically connected by a high density connector assembly.

The cassette body can also be broken down into cold end and warm end structures. The cold end structure is broken down into several sub-assemblies: namely the "feed-through assembly", the G-10 walls, the heat "intercept" assemblies and the cold

end copper cup (see Fig. IV-1). Along the length of the cold end, two heat intercepts are integral to the cold end cassette structure. The first is the liquid nitrogen intercept (77 Kelvin) which serves to cut off the flow of heat from the warm end. The second is the liquid helium intercept, with a name more historic than functionally descriptive, which serves as an IR suppression device and terminating structure. The warm end structure is mad of parallel aluminum plates spaced by spacer bars which form a protective box for the optical bundles.

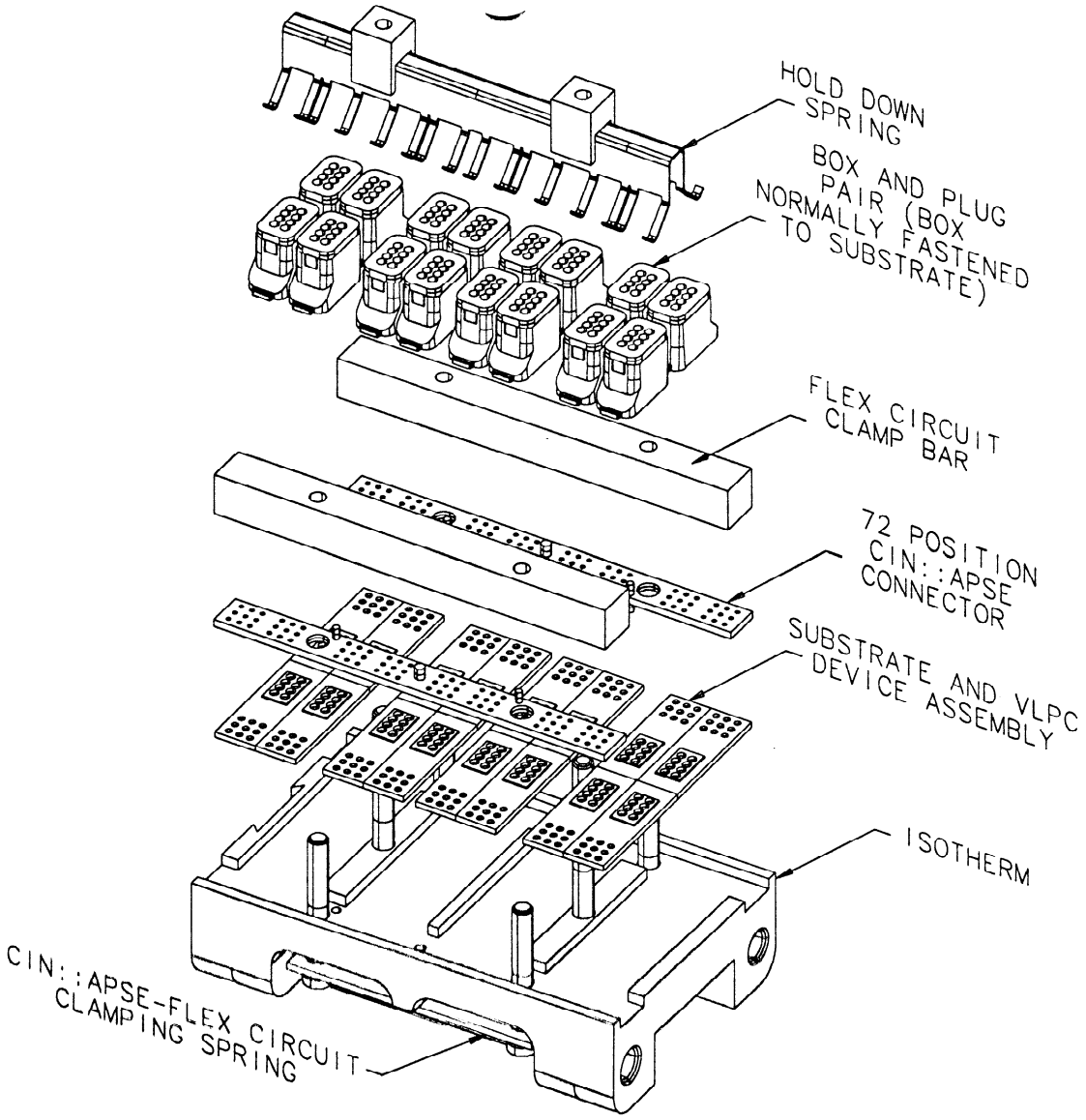

Figure IV-3 Cold-end assembly for one 128 channel module of the VLPC cassette.

An important subassembly of the warm structure is the "warm end Cinapse connector mechanism", the mechanism which connects the flex circuits to the read-out electronics boards. The readout electronics boards, used as interface between the cassettes and the data acquisition system, are also considered to be part of the warm end structure with regards to mechanical layout. The cassette is mounted to the cryostat top plate at the "feed-through assembly". This assembly provides a gas tight compression

fitting which provides a seal to the cold, inert ² 2 psig stagnant helium volume within the cryostat. At the center of the cassette are eight 128 channel fiber optic bundles, modular bundles of optical fiber which run from the top to the bottom of the cassette and pipe the optical signal coming from the detector to the VLPC. An optical bundle includes a warm end 128 fiber molded epoxy connector, a urethane block for sealing at the feed-through assembly, two Kapton flex circuits, and is terminated with sixteen Ryton optical "plugs" which mate with matching "boxes" which are adhesively bonded to VLPC hybrid assemblies.

IV.4 Cryosystem

Since the VLPCs operate at cryogenic temperatures, a liquid Helium cryosystem is

required. The VLPCs will share the Helium refrigerator with the solenoid magnet and the VLPC cassette cryostats will operate off a separate control dewar. Two cryostats, each accommodating up to 51 VLPC cassettes, will house the entire VLPC system. Two cryogens are used in the system. Liquid Helium from the control dewar will allow for VLPC operation down to 6 K and liquid Nitrogen will cool an intermediate heat intercept in the VLPC cassette (described above) in order to reduce the heat load to the liquid Helium. The cassette cold end will sit in a stagnant gaseous Helium volume. Conduction through the gas will cool the VLPCs. The prototype cryosystems used in VLPC testing maintained the VLPC set temperature to within 50 mK. The specification for the final Central Fiber Tracker VLPC cryostats is also 50 mK.

IV.5 References

[1] "DØ Fiber Tracker 1024 Channel VLPC Cassette Technical Design Report and Specification"

[2] M.D. Petroff and M.G. Stapelbroek, IEEE Trans. Nucl. Sci. **36**, No. 1(1989) 158. M.D. Petroff and M.Atac, IEEE Trans. Nucl. Sci. **36**, No. 1(1989) 163.

Chapter V. Readout Electronics

V.1 Overall Design

The CFT readout electronics are contained on three sets of printed circuit boards which are located at three different places, as shown in Fig. V-1. The front end boards digitize the signals and form the trigger tracks. These boards are mounted directly on the VLPC cassettes and come in two varieties, stereo and trigger boards. The Port Card Boards read out the digitized values from the SVX chains and transmit them via fast optical link to the third set of boards, the VME Readout Buffers, VRB. The Port Card Boards are located in the center platform of the detector in the collision hall and the VRBs are located in the moving counting house. Both the Port Card Boards and VRBs are identical to boards used by the D^- silicon tracking electronics.

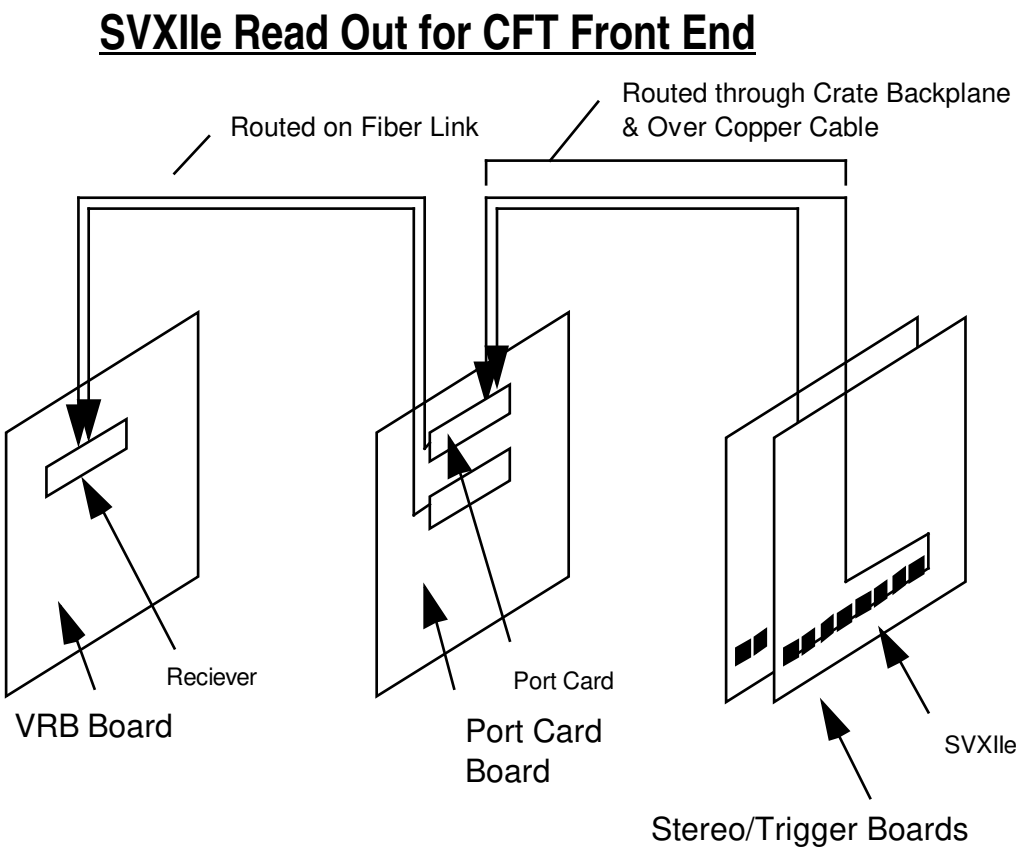

Figure V-1 Overall layout of the read out system. The analog signals are digitized in the SVX IIe chips located on the stereo/trigger boards on the right. The digitized and zero suppressed data is read out of the chain of SVXs by a

port card located on the port card board via a copper link. The data is then transferred to a VRB in the moving counting house over a fast serial link.

The front end boards receive the analog electrical signals from the VLPC cassettes split them and store one part of the signal in a 32 deep pipeline buffer. On receipt of a level 1 accept one of the stored events is digitized using the SVX-IIe chip and transferred over a fast serial link to the moving counting house where it is available to the DAQ system. On the trigger boards the other part of the analog signal is discriminated using the SIFT-2b chip and the discriminated outputs are used to form a pre level 1 axial track list. This list is transmitted to other detector parts for use in level 1 triggers and is also pipelined for transmission to the level 2/3 on a level 1 accept.

V.2 Interface to VLPC cassette

Each cassette holds two front end boards which are slightly different versions of the same board. The board mounted on the right side of the cassette when viewed from the front is called the Right Hand Board, RHB, and the one on the left the Left Hand Board, LHB. Each front end board supports 512 channels of signal from the cassette. The RHB (but not the LHB) interfaces to the cryogenic power and controls system for each cassette. Each front end board interfaces to the bias voltage supply and return for the VLPCs.

The CFT is divided into eighty equal wedges in azimuth known as sectors. The channels from each sector are input into two front end boards. The channels from the stereo fibers are input into the stereo boards. The channels from the axial fibers are input into the trigger boards which also contain the logic which forms the level 1 axial trigger tracks. While each board supports 512 input channels the CFT will not use them all. On each trigger board 480 of the 512 channels are used by the CFT. On each stereo board, only 448 channels are used by the fiber tracker. The remaining channels are used by the Central Preshower Detector (CPS).

The crate back plane for the front end boards is mounted on the cryostat within a rigid structure spanning the length of the cryostat. When the cassettes are inserted into the cryostat they also mate with this structure and form a VME type crate which is 9U high and 250mm deep. All of the crates have a back plane which connects the front end boards with the port card boards, the serial control link and to the cryogenic control. One-half of the crates are trigger crates, which have two additional back planes used to pass the fiber signals between neighboring front end boards in order to form a seamless

trigger. The trigger cassettes are in one contiguous section of cryostat and the stereo in another.

The signal connection between each front end board and the cassette is made along the bottom edge of the board. See figure V-2. Eight sets of pads are located along this bottom edge which mate with the high density connector pins of the Cinapse connector . Each of these eight sets includes 64 pads which are the single ended signal outputs from the VLPCs. Each of these lines is AC coupled through an isolation capacitor to the input of the front end electronics. These 64 lines are also the return lines for the VLPC bias current and are DC coupled through a resistor to a common VLPC bias return. Eight of the pads are connected to a common VLPC bias supply which supplies the bias current to the VLPCs. Six of the pads are connected to the cryogenic controls for the cassette.

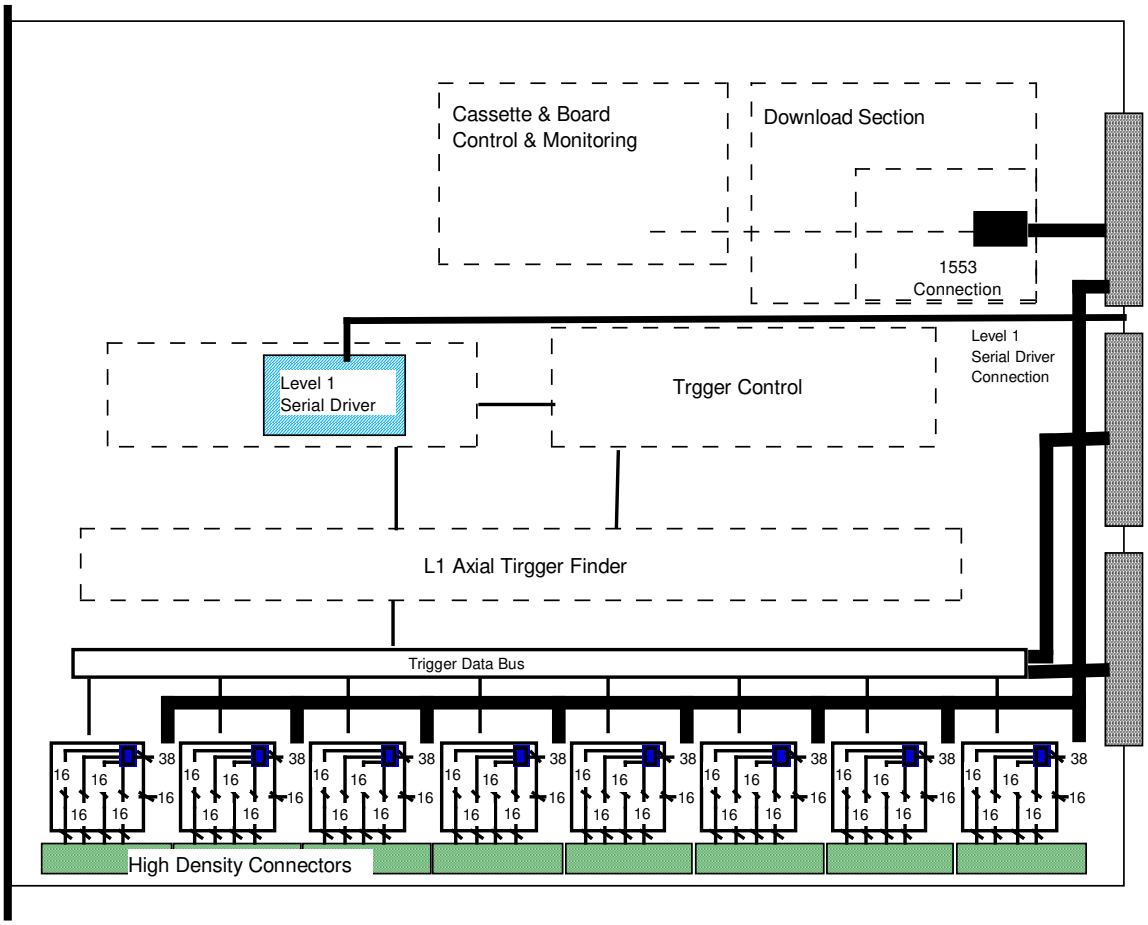

Figure V-2 Schematic of a front end board trigger boards for the CFT. The blocks along the bottom edge are the pad arrays which mate with the Cinapse connectors. Directly above them are the eight multi-chip modules, MCM, each of which contains four SIFT-2b chips and one SVXIIe chip.

V.3 Front end electronics

V.3.1 Front end electronics

A sketch of the front end electronics for one trigger channel is shown in figure V-3. The box on the left represents the VLPC. Its DC bias voltage is supplied by modified D0 high voltage modules located in the moving counting house. For this application they supply from 5 to 8 volts. Each cassette has an independent supply. The output signal from the VLPC is superimposed on the bias return line so the two must be separated. A capacitor is used to couple the output signal to the electronics. There is one discrete capacitor for each channel mounted directly on the front end board for this purpose. In a common failure mode for a VLPC cell its internal resistance drops to 0 Ohms. When this happens the current increases and heats up the failed VLPC cell. This heat produces infarred light which can swamp neighboring cells within the 8 cell VLPC chip with noise. To protect against this a large resistor is mounted on the PC board for each channel.

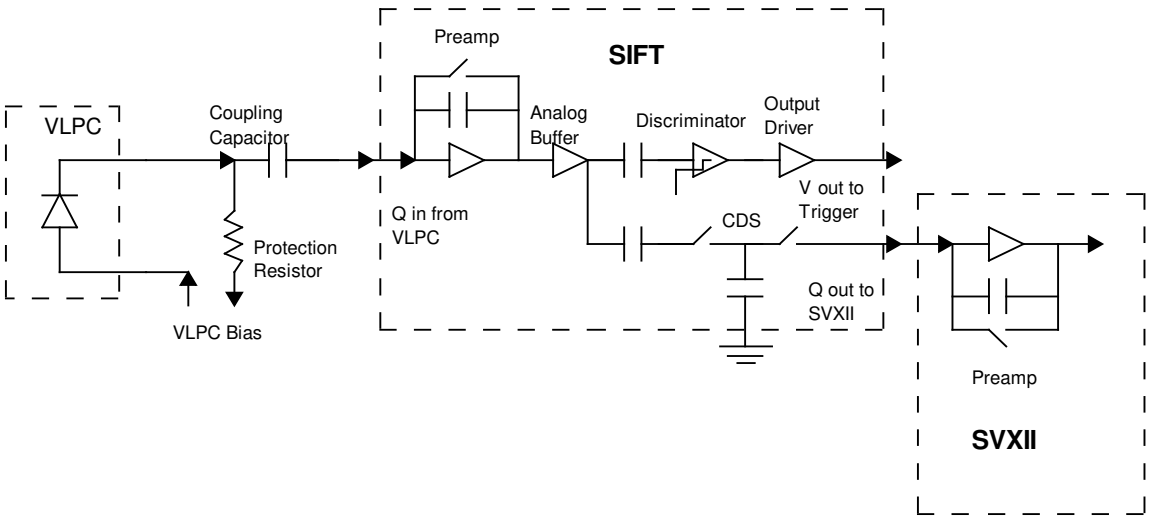

Figure V-3 Electronics schematic for one channel of the trigger board. The VLPC is represented by the small box on the left. The analog signal is separated from the bias current by the coupling capacitor. This capacitor is a discrete part mounted on the PCB. The next two boxes represent the circuit inside the SIFT-2b chip and the first part of the SVXIIe chip respectively.

V.3.2 Digital Pick off for Trigger

A fast logical output is need for any channel used in a level 1 trigger. For the Central Fiber Tracker this is done by placing a chip in the analog signal line after the coupling capacitor and before the SVX chip. The SIFT chip[1] was developed within D^- for this application. Each SIFT chip has 16 input channels and a common threshold. The chip first amplifies the signal and then buffers it. In two different time slices it then discriminates each input signal and outputs a 3.3V single ended output for those channels above threshold, and for every channel the SIFT chip outputs an analog signal to the SVX for digitization.

V.3.3 SVXII Readout

The SVXII chip[2] and its readout support were designed for the silicon tracker but are well suited to the fiber readout as well. The signal amplitude and shape as well as the effective detector capacitance out of the VLPC or SIFT are well within the range of the SVXII chip. While eight bits of digitized amplitude may not be strictly necessary for the fiber channels there are considerable savings in development and maintenance by sharing the readout for the 78,000 channels of the CFT with the over 300,000 channels of the D0 silicon vertex tracker. Detailed information on the silicon tracker read out system can be found in several places[3] and will not be repeated here. The following will repeat some of the general features and highlight the differences for the fiber system.

The SVXII read out system has three parts. The first part is the digitization which is the SVXII chip itself. This is connected via copper bus to the port card which is the read out part. This in turn is connected via fast optical link to the VME Buffer Driver, VBD, which collects and stores the data for VME based readout by the DAQ system. The SVXII chips are located on the front end PCBs. The port cards are located in a separate set of crates in the platform among the port cards for the silicon tracker. The

VBDs are located in the movable counting house, again among those for the silicon tracker.

Each front end board has eight SVX chips. Each of these chips will have one-half of its 128 input channels connected to VLPC outputs. The SVXII chips are read out in chains of chips. When a level 1 accept is received all the chips stop accruing data and transfer the data from one of their analog memories to the digitization stage. When the first SVX on a chain has finished its digitization it starts transmitting data to the port card. After the first SVX has finished its data transmission the next chip in the chain is then free to transmit. Since the SVX chips will be run in zero suppression mode only those fibers for which the signal was above a threshold will be read out. Thus, the total read out time is a function of the occupancy of the fibers for each of the chips in a chain. Given the expected occupancy for the CFT and the available readout time, the eight SVX chips on each PCB are arranged into two chains. Each pair of two chains are connected to one port card which sends the data via a single, fast serial, optical link to the VRBs.

V.4 References

[1] "A Custom IC for Visible Light Photon Counters", S. Mani et al. (private comm.); "Testing the SIFT with the ADAPTER Board", F. Borcherding, FNAL (private comm.)

[2] "A Beginners Guide to the SVXIIE", R. Yarema et al., Fermilab-TM-1892, June 1994 (revised October 1996)

[3] "DØ Silicon Tracker Technical Design Report", DØ Note 2169, July 1994; "SVX Sequencer Board", M. Utes, DØ Engineering Note 3823.110-EN-480, November 1997.

Chapter VI. System Test

VI.1 Overview

For most of the time period between May 1994 and June 1995, the DØ Fiber Tracking Group operated a large-scale system test measuring cosmic rays with a prototype scintillating fiber tracker with VLPC readout. This test represented the first operation of large numbers of Visible Light Photon Counters (VLPC). The goals of the test were to: 1) demonstrate that a fiber tracker with a configuration similar to the detector which will be implemented into the DØ upgrade can detect minimum ionizing particles with high efficiency and good position resolution, and 2) demonstrate that a VLPC-based readout system can be operated stably over a significant period of time.

In this section we will limit ourselves to a brief discussion of the test setup and results. More details on the cosmic ray test can be found in a number of published reports [VI-1,2,3].

VI.2 Cosmic Ray Test Stand

Two different detector configurations were operated during the system test. The first configuration was a prototype of the DO fiber tracker and contained a total of 3,072 scintillating fibers arranged in three superlayers. One superlayer was mounted at the top of a 20 inch diameter, carbon-fiber support cylinder. A second superlayer was mounted at the bottom of the cylinder, 180^o opposite the first superlayer. The third superlayer was supported on a flat carbon-fiber board along the cylinder axis. Each superlayer was made up of 4 doublet ribbons of scintillating fibers, each 128 fibers wide. Two of the four doublets in each superlayer had their fibers oriented parallel to the cylinder axis, while the other two doublet layers were oriented at $\pm 2^o$ stereo angles.

Although several important results were obtained with this first fiber configuration, a flaw in the ribbon construction prevented us from obtaining the position resolution predicted for the prototype. To correct this, the initial prototype fiber tracker was replaced with a second, smaller setup totaling 1,785 fibers. This new detector contained a total of 7 fiber doublets mounted on three flat boards, with all doublets oriented in the axial direction.

Both detector configurations were located above a 2 meter high stack of steel. Trigger counters above and below the steel selected cosmic ray muons with a minimum momentum of about 2.5 GeV/c.

The fibers were read out with the HISTE-IV version of VLPC. The 3,072 channels of VLPC were located in 24 cryogenic cassettes of 128 channels each, which were all housed in a single cryostat for operation. All channels were operated at a temperature of 6.5 K and a bias voltage of 6.5 V. Signals from the VLPC pixels were input to the QPAO2 preamplifier. The outputs of the QPAO2 were digitized by LeCroy 1885 ADCs.

VI.3 Results

VI.3.1 Data sample

Totals of 18.2 million and 9.9 million cosmic ray triggers respectively were taken with the 3,072 channel prototype and with the second apparatus designed to measure position resolution. In addition, several millions of both calibration and random noise triggers were taken throughout the running period. The VLPC cryostat was warmed up and cooled back down to operating temperature a total of 5 times during the run.

VI.3.2 Photoelectron yield and efficiency

After calibrating each VLPC channel to determine its gain, the average response of a fiber to a cosmic ray can be determined. A fit to the cosmic ray pulse height spectrum gives a mean value of 9.6 photoelectrons per fiber. This is approximately a factor of four larger than the minimum number of photoelectrons required for an efficient fiber tracking system.

Singlet and doublet layer efficiencies were determined by finding cosmic ray tracks, excluding the layer under study, and then extrapolating the track to the layer under study to see if either of the closest fibers nearest the track were hit. The efficiencies were measured for a variety of thresholds, where the threshold on each channel was set to maintain the single channel noise rate at a given value. Both the singlet and doublet efficiencies are given below in Table VI-1. The singlet efficiencies on the order of 85% reflect the geometric efficiency of a single fiber layer. Excluding regions containing dead channels, the doublet layer efficiency was $\geq 99.5\%$ over a range of thresholds for which

the probability of a noise hit within the 100 nsec readout gate varied from 0.125% down to 0.025%.

VI.3.3 Position resolution

The position resolution was measured using the four innermost fiber doublets in the second, 1785 fiber test configuration. Points in the top and bottom doublets were connected by a straight line fit, and the residuals to this line were determined for the four inner doublets. The resolutions for doublets 3-6 are given in Table VI-2 below, along with the predicted resolutions using a GEANT simulation. The resolutions for doublets 5 and 6 are within a few microns of the prediction, while the resolutions for doublets 3 and 4 were 10 and 30 microns worse than expected, respectively. It is believed that this discrepancy is due to slight variations of the ribbon position along its length for these two doublets.

Table VI-1
Singlet and doublet efficiencies

Noise level in %	Singlet Efficiency	Doublet Efficiency
0.025	83.5 %	99.5 %
0.050	83.9 %	99.5 %
0.075	84.4 %	99.5 %
0.100	84.6 %	99.6 %
0.125	84.8 %	99.6 %

Table VI-2
Position resolutions for doublets 3-6

Doublet	Geometric Monte Carlo	GEANT Simulation	Measured Resolution
3	90 μm	90 μm	101 μm
4	91 μm	101 μm	132 μm
5	91 μm	101 μm	104 μm
6	91 μm	91 μm	92 μm

VI.3.4 Stability of VLPC operation

By taking large numbers of calibration and randon noise triggers throughout the run, the stability of the VLPC readout system was monitored over a period of nearly 300 days. We measured the following quantities for all channels: the VLPC gain, the gain dispersion (defined to be the percent difference, in quadrature, of the pedestal and 1st photoelectron peak widths), and the threshold required to keep the noise rate at 0.1% and 0.2%. All of these quantities were stable to better than 1% over the entire running period.

VI.4 References

[1] D. Adams et al., IEEE Trans. on Nucl. Sci. **42** (1995), 401.

[2] B. Baumbaugh et al., IEEE Trans on Nucl. Sci. **43** (1996), 1146.

[3] B. Baumbaugh et al., Proceedings of DPF 96, Minneapolis, MN (to be published).

Chapter VII. Fabrication and Assembly

VII.1 Scintillating Fiber Ribbons

VII.1.1 Fiber Quality Control

Before the scintillating fibers are assembled into ribbons, a small percentage of each fiber shipment from Japan will be brought to Notre Dame for tests and long-term storage. Each fiber to be tested will be placed into a dark box. Blue LED light will be used to excite the fiber and monitor its performance. The LED light source is under computer control and will scan the length of the fiber to measure both total light output and attenuation length. The test fibers will be read out into a special, 32-channel VLPC cassette designed to operate in a flow cryostat. The diameter control of the test fibers will also be checked with the use of a laser micrometer. After testing, the fibers will be stored and periodically re-measured in order to monitor their long term stability.

VII.1.2 Fabrication Technique

Individual scintillating fibers are combined into ribbons containing 256 fibers each, before being attached to carbon fiber support cylinders in the DØ fiber tracker detector. A ribbon has two single layers of 128 fibers offset from one another by 1/2 fiber pitch. Ribbons are fabricated by placing one layer of 128 fibers into a grooved mold, applying a layer of polyurethane resin, adding the second layer of fibers and compressing the assembly while the resin cures. One end of each fiber is polished and silvered before ribbon fabrication to form a reflective surface at the far end of the ribbon. The other end of each ribbon is mass terminated with an optical connector.

A ribbon mold consists of a flexible sheet of 1/16 inch thick Delrin plastic containing a parallel array of machined v-grooves, which is attached to a curved aluminum suppport having the correct radius for a particular layer of ribbons in the detector. The basic idea is illustrated in Fig. VII-1. A Thermwood machine at the Lab 8 routing facility at Fermilab is used to cut the grooves and exterior edges of the Delrin. The cutting tool for making the grooves is a square end mill rotated 45 degrees from the plane of the Delrin. The end mill has a 10 mil wide flat at 45 degrees on its corners. This setup generates flat-bottomed v-grooves with a 90 degree included angle. When fibers are laid in the grooves, the gap to the bottom of the grooves is typically only 0.002-0.003 inch. The flat bottom on the mold grooves limits the thickness of the layer of resin that

flows down under fibers and makes the ribbon thickness more uniform. Pitch uniformity on molds machined with this process is somewhat better than the overall specified 25 μm rms circumferential accuracy of fiber placement on a cylinder. Since the Thermwood machine does not have a rotational degree of freedom, the Delrin must be cut in a flat state, and then curved and affixed to a rigid support. An adjustment is required in the flat machined pitch in order to achieve the correct ribbon pitch in a curved mold. The mold has 129 grooves. A single scintillating fiber is epoxied into an edge groove, and becomes a permanent part of the mold. This serves as a support for positioning the overhanging fiber on the upper layer of a molded ribbon.

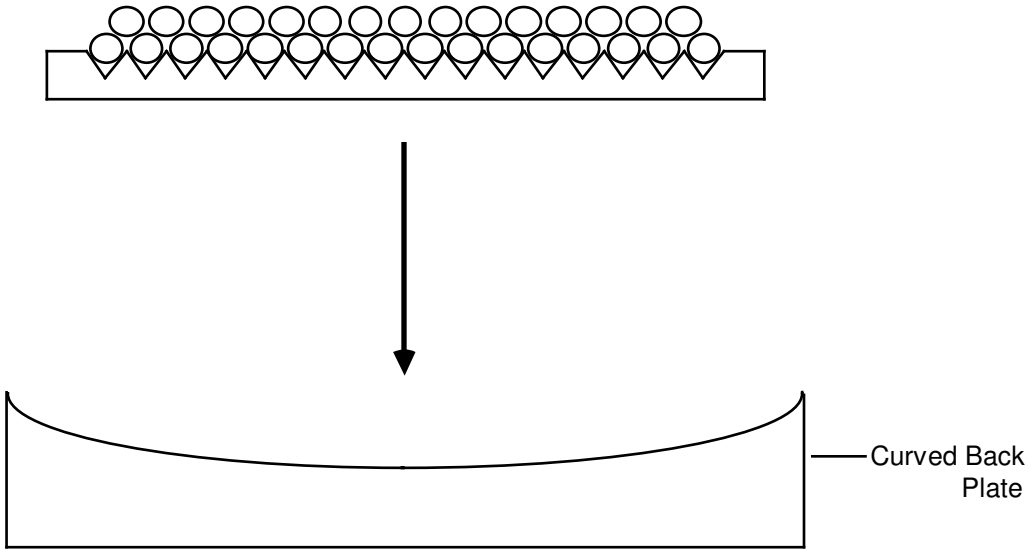

Figure VII-1 Technique for curved scintillating fiber ribbon fabrication.

The molding process involves first cleaning and then coating the mold surface with Mann type 315 silicone mold release. The primary purpose of the mold release is to aid in the extraction of a cured ribbon, but it also helps to hold the first layer of fibers in place during assembly. A single layer of 128 fibers is placed into the mold grooves. Then a layer of Ciba Geigy type 6400-1 polyurethane is applied to the bottom layer of fibers. Soft tools are used to spread the urethane to a thickness that is about even with the top of this layer of fibers. Then the top layer of fibers is laid into the resin between fibers in the bottom layer. A sheet of mold release film is placed over the assembly, followed by a 1/2 inch thick layer of soft sponge rubber and a top plate. The entire assembly is clamped together to provide a pressure of about 1 psi on the ribbon during curing. The

applied resin flows into the finished assembly to mostly fill the grooves in the mold and to form interfiber fillets slightly above the midplane of the upper layer of fibers. The amount of applied resin is approximately 10-15% of the weight of the fibers. The resin chosen for the ribbons has a nominal hardness of Shore A 52. Its relatively low hardness produces a flexible ribbon that can undergo routine handling without overstressing the bond to the fiber surfaces. Ribbons can typically be demolded within 5 hours.

After all of the ribbons for a particular layer have been fabricated, the mold assembly will then be transferred to the ribbon laying machine, where it will become a part of the process of attaching ribbons to a support cylinder. The overall radial uniformity for the ribbon laying machine is required to be within a few thousandths of a inch, and circumferential accuracy is required to be better than +/-0.001 inch. These tolerances then demand a correspondingly tight tolerance for the mold structures. The thickness variation of the machined Delrin is expected to be about +/-0.002 inch, and +/-0.001 inch accuracy is specified for the thickness and cylindrical surface of the aluminum substrate. The aluminum substrate attaches to a rigid steel beam which has a ground surface that is flat within +/-0.001 inch. These tolerances, in combination with tolerances in the rest of the ribbon laying machine and in the laying process, should give an overall radial accuracy of +/-0.003 inch. This radial error translates to a total circumferential error of about +/-0.020 inch in the worst case. A nominal inter-ribbon gap, typically 3-6 mils, is included to accomodate this total error. The innermost cylinder is the worst case, for this problem, because it has only 10 ribbon gaps around its circumference.

VII.1.3 Ribbon Measurement

Once the scintillating fiber ribbons have been fabricated it is essential to measure the completed ribbon to verify the accuracy of the fiber placement. A machine utilizing a ^{57}Co s-ray source has been designed to perform this measurement, and is currently under construction at Fermilab. The purpose of the machine is to measure the fiber's position in curved ribbons with an accuracy of 0.001" rms or less. The machine has been designed to measure both the axial and stereo ribbons, and will allow the ribbons to be measured in any of the following stages: 1) right after the ribbon has been made and before it is taken out of the mold, 2) after it is taken out of the mold, and 3) after the ribbon is put in the holder of the ribbon laying machine. Since the fibers will be excited using an x-ray source there will be no need to leave exposed fibers for a touch probe or similar device. Also, if deemed necessary, this machine could be adapted with minor modifications to

measure fiber positions once the ribbons have been mounted onto their carbon fiber support cylinders.

A detailed study of the feasibility of using ^{57}Co for this procedure has been carried out [1]. Figure VII-2 shows the basic principle. A collimator limits the x-rays to within a narrow beam, and as the source is scanned across the fiber ribbon the light output from individual fibers mirrors the position of the source. Thus an accurate determination of the source position translates to an accurate knowledge of each individual fiber location. Since the x-rays are very penetrating, several layers of fibers can be measured at the same time independently of the way the ribbons are fabricated. Figure VII-3 shows an engineering sketch of the ribbon testing apparatus, with the x-ray source moving on a curved rail located just above the fiber ribbon in its curved mold.

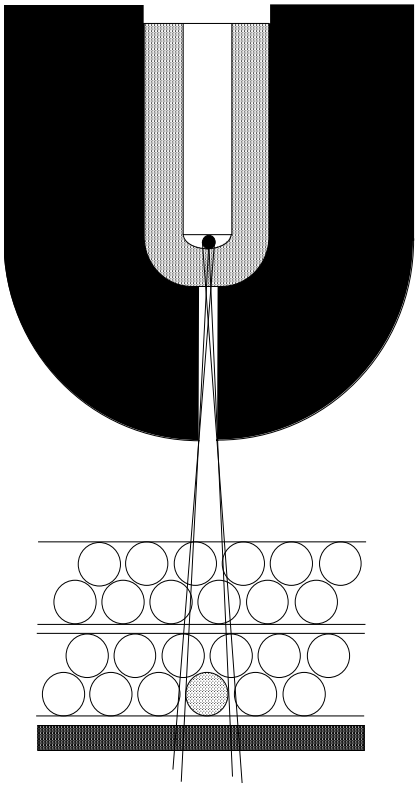

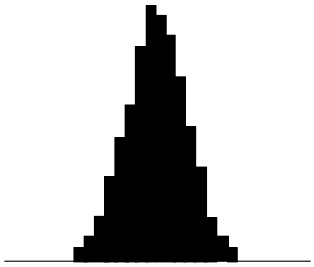

Figure VII-2 Illustration of ^{57}Co x-ray method for measuring the accuracy of scintillating fiber ribbons.

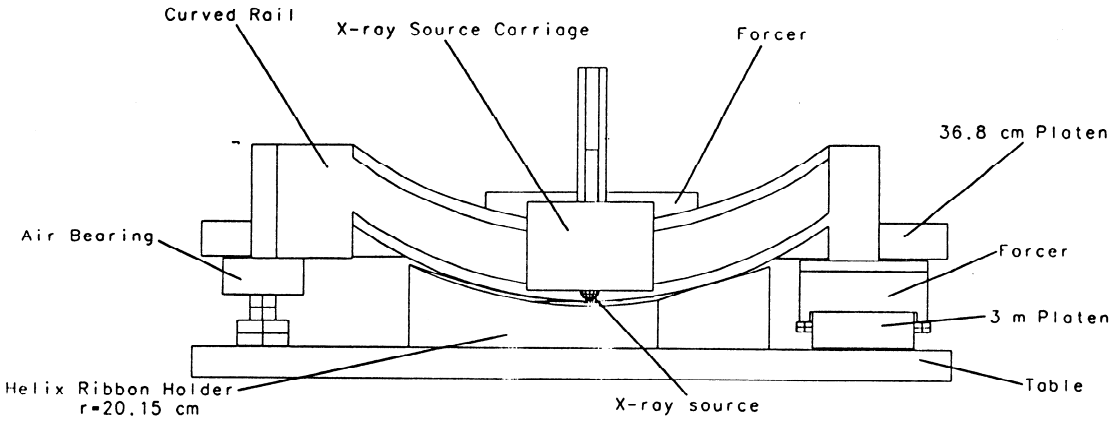

Figure VII-3 The ^{57}Co x-ray fiber ribbon measuring apparatus. The x-ray source moves curved rail above the fiber ribbon.

VII.1.4 Ribbon Connectors

For the DØ detector a v-groove connector design has been adopted. There are a unique set of connectors for each doublet fiber layer, since the connector must be made with the correct curvature for a given layer on a given support cylinder. The curved connectors are attached directly to the end of the fiber ribbons, with no "flying leads" of fiber necessary. The connectors are attached directly to the end rings of the carbon fiber support cylinders as the ribbons are mounted into place. Each 256-fiber clear waveguide bundle will also terminate in a matching connector. The design provides a method of

connecting the scintillating fibers to the clear waveguide fibers with high precision and good light transmission (~ 92% dry, ~ 95% with mineral oil or optical grease), and allows the scintillating fiber ribbon to be registered over its entire length.

VII.1.5 Ribbon Mounting

A special ribbon mounting machined has been designed to place the scintillating fiber ribbons onto their carbon fiber support cylinders with the required precision. The machine will work in conjuction with a large (3m x 3m x 1.5 Coordinate Measuring Machine (CMM) purchased for the CFT project. In the mounting procedure each ribbon, in its mold and curved backplate, will be secured to a rigid beam which is located below the carbon fiber support cylinder. The CMM insures that the ribbon mold and the cylinder are oriented correctly with respect to each other. The beam is raised up to the cylinder surface and the ribbon glued onto the cylinder. Once the glue sets and the ribbon is securely attached to the support cylinder, the beam is retracted so that the next ribbon can be placed into the mold. The mounting machine then rotates the support cylinder the correct angular distance to allow the next ribbon to be brought back up and glued adjacent to the previous ribbon. The procedure is continued until all the ribbons on a given cylinder are mounted. Once the axial doublet layer is mounted, the procedure is repeated for the stereo layer. The mounting machine has been designed so that all ribbons can be place on all eight support cylinders with minimal modification to the machine.

VII.2 Support Cylinders

VII.2.1 Specifications

To achieve the required momentum and vertex resolution the error in the radial position of the fibers has to have an rms of σ^2 0.006 inches. To achieve this the fiber ribbons can be placed on the carbon cylinders in two different ways:

Option 1: The carbon cylinder determines the radius at which the scintillating fibers are placed. In this case the fibers are attached to the cylinder in such a way that they follow the shape of the cylinder. Then the error in the radius of the cylinder has to have an rms of [ ] inches.

Option 2: The scintillating fibers are mounted in the cylinder placing the fiber ribbons on an accurately built rigid mold. Then the mold is brought close to the cylinder but without touching, therefore the radius is determined by the distance from the rigid mold to the axis of the cylinder. This distance can be controlled to 0.001 inches. Therefore errors in the cylinder radius only add to the amount of glue needed to attach the ribbons to the cylinder.

Tests performed with the polyurethane glues currently in use, and the current ribbon fabrication techniques, have shown that gaps between ribbons and carbon fiber cylinders ranging from 0 to 0.015 inches allow ribbon mounting to the required precision.

The current design of the ribbon mounting machine uses option 2, therefore the carbon cylinders should have all deviations from their nominal radius limited to within a band of 0.015 inches.

VII.2.2 Optimization of mass

The current plan is to make all eight cylinders out of high-modulus carbon fiber. Among other possible fabrication materials, only beryllium can produce cylinders with equal rigidity and less radiation length than carbon fiber, but the amount of beryllium needed for the eight fiber tracker cylinders is prohibitively expensive.

Two way of building cylinders were tried: 1) single-wall cylinders, and 2) double-wall cylinders. The single-wall cylinders are made with just a wall of resin-impregnated carbon fibers. The resin amounts to about 40% of the total weight. In a double-wall cylinder a core of foam or honeycomb is used in between two layers of carbon fibers. Both type of cylinders have been fabricated and measured at Fermilab, and after careful study a consensus was reached to make the support cylinders for the CFT of a double-wall construction.

The amount and modulus of carbon fibers needed is basically independent of the cylinder being single or double-wall. Under the load of the scintillating fibers, plus their own weight, the smaller radius carbon cylinders (cylinders 1-3) deflect in such a way that the cross section remains circular. In this kind of deformation, known as beam deflection, the sagging occurs by stretching the bottom and compressing the top. Therefore as long as the wall thickness of the cylinders is small compared to the radius the deflection is the same for single or double wall cylinders. ANSIS calculations show that to achieve a maximum of 0.001 inch beam deflection in the small radius cylinders a thickness of 0.016 inches of high modulus carbon fibers (100 mpsi) is needed. As the cylinders increase in radius the beam deflection becomes smaller and lower modulus

carbon fibers can be used (even though for stability reasons this may not be a good idea). Under loading, the large radius single-wall cylinders (cylinders 6-8) do not remain round. This precludes the possibility of reducing the wall thickness instead of reducing the fiber's modulus. If the double-wall construction is used the local stiffness is greatly increased and the large radius cylinders remain round when loaded. But in this case reducing the wall thickness becomes very difficult because the two walls on each side of the core, with a thickness of 0.008 inches, are already very thin.

The mass is minimized when single wall-cylinders are used, but since they have very little local stiffness they are very sensitive to axial loading and temperature and humidity changes. In the current construction of double-wall carbon cylinders we are using a Rohacell 31 core, which is the lowest density available. The thickness of this core is 0.25 inches and in terms of radiation lengths is equivalent to 0.005 inches of carbon fiber. What is gained with this increase in mass is a very large increase in local stiffness, which translates into a gain of about a factor of five in stability with respect to axial loading or temperature and humidity changes.

The mass of the double-wall cylinders is 0.18 % of a radiation length for the carbon fibers (assuming a 40% resin content) and 0.06 % for the rohacell core. Unless the deflection and stability requirements are relaxed this total of 0.24% of a radiation length is the minimum amount of material that can be achieved.

VII.2.3 Cylinder lay-up and fabrication

The carbon cylinders were constructed using linear carbon fibers impregnated with about 40% resin. ANSIS calculations show that the best lay-up to minimize the sagging of the cylinders is: 0û/60û/-60û/core/-60û/60û/0û. The numbers are the angles in degrees of the carbon fibers with respect to the axis of the cylinder. Given that the total carbon fiber thickness is 0.016 inches, each layer must be about 0.0025 inches thick. The carbon fiber impregnated with epoxy that was used for the R&D phase was 0.004 inches thick. Therefore a lay-up of 45û/-45û/core/-45û/45û was used for the R&D cylinders fabricated with that material.

The R&D cylinders were fabricated on a steel mandrel. As an example, the procedure used for a 12" diameter, 80" long cylinder is as follows. The layup, from the mandrel to the outside, was: 1) 12" steel mandrel, 2) silicon based mold release, 3) 45û and -45û inside carbon layers, 4) 0.25" rohacell 31 core, 5) -45û and 45û degree outside carbon layers, 6) release fabric, 7) rubber caul sheet, 8) breather material, and 9) nylon vacuum bagging. The cylinder was then cured in an oven with the following cycle: 1)

apply vacuum to the cylinder, 2) raised temperature to 250 degree Fahrenheit at about 3 degrees/minute, 3) hold temperature at 250 degrees for at least one hour, 4) turn off oven and electric heaters, 5) wait for at least 8 hours, 6) release vacuum and take the cylinder out of the oven.

VII.2.4 Measurements

The cylinders were measured in a CMM. Measurements were made on the outside surface of the cylinders every 22.5 degrees around the circumference and every 2" along the axis. A perfect cylinder was then fit to the data, and deviations from the perfect cylinder were calculated. The rms of the deviation for the 12" diameter by 80" long cylinder is 0.0031 inches, well within the required cylindricity. Figure VII-4 shows the average of the measurements made along the axis as a function of the angle around the circumference. The scale of the plot is such that 1 division corresponds to 0.00625 inches. The (slightly) oval shape may be due to residual stresses in the rohacell core. This is now under investigation.

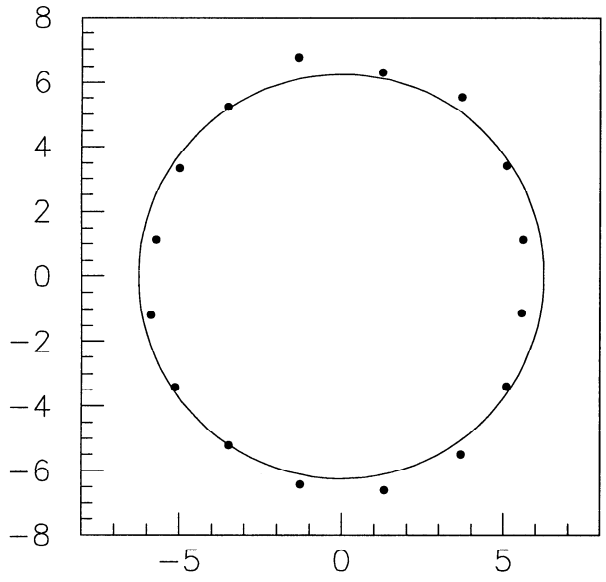

Figure VII-4 Average deviations from a cylindrical fit for the 12" diameter, 80" long double-wall R&D cylinder fabricated at Fermilab. One division equals 0.00625 inches.

VII.3 Support Cylinder Assembly

To assemble the CFT, all eight support cylinders will be aligned and mounted together with the aid of a large CMM. In the current assembly scheme, once they are accurately aligned, successive cylinders will be interlocked together by thin, carbon fiber annular rings which connect the inner surface of a given cylinder's end ring to a flange mounted on the outer surface of the cylinder immediately inside. Figure VII-5 shows a detail of the end rings, flange and annular connecting piece for cylinders 4 and 5. The design for connecting cylinders 2 to 3 and cylinders 3 to 4 is slightly different due to the change in cylinder length starting with cylinder 3. This solution is attractive because of the relatively low mass and even distribution of the support structure involved. However, questions of long term effects of mechanical pressure on scintillating fibers still have to be answered for this support and connection scheme before this design is finalized.

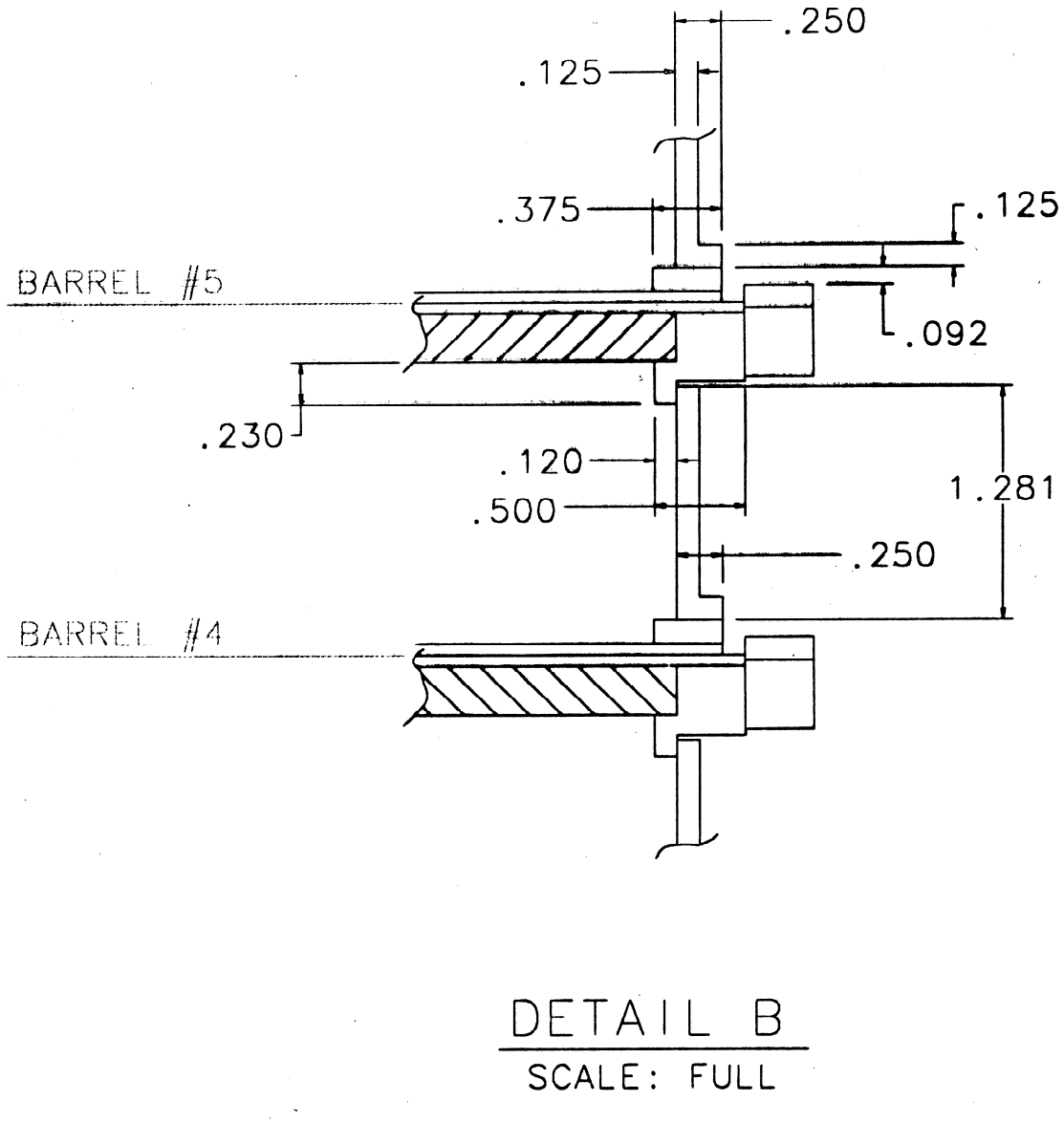

Figure VII-5 Detail of the support cylinder interconnections for cylinders 4 and 5.

VII.4 Clear Waveguide Fiber Bundles

VII.4.1 Fabrication techniques

As a part of the fiber tracking collaboration, University of Illinois at Chicago (UIC) made 30 128-channel lightguide bundles, either 8 m or 11 m long, employing some

20 miles of fiber. Twenty-four of them have been successfully used in the 3000 channel system test . Each of the bundles was assembled with two 128-channel holed square-shape connectors made by machining black Delrin plastic. The details of the bundle fabrication can be found in Ref. [3].

The old bundle making process is briefly described here. It began by inserting a pair of degreased connectors in their holders. Then, an appropriate length of fiber was unwound from the fiber spool and cleaned with ethyl alcohol using lint-free wipes. The fiber used for these waveguide bundles was clear, multiclad fiber manufactured in Japan by Kuraray [4]. After all connector holes were filled, the connectors were removed from their holders and inserted into another pair of fixtures for epoxying. These fixtures held the connectors in a horizontal plane with the fibers emerging vertically. For gluing ends of lightguide fibers in the connectors, Bicron [6] BC-600 epoxy was used because of its high strength and because it is specially formulated for gluing plastic fibers [7]. After allowing the epoxy to cure for about 24 hours, the fibers were enclosed in a black PVC jacket manufactured by the Zippertubing Co [8]. The jacket served to protect the fibers and keep them physically together. To reduce the likelihood of breaking fibers at the connectors due to handling, aluminum strain reliefs were attached at both ends of the bundles. After the construction of the fiber bundles was completed, all connector faces were polished on a special facing machine employing a diamond-tipped fly-cut tool that was dubbed "P-3" at Fermilab [9]. Each of the bundles fabricated was tested for light transmission, both to validate the fabrication procedure and to check the quality of the Kuraray fiber. Excluding one bundle that appeared to be damaged in handling, the bad channel frequency was found to be 0.2% for all 3712 channels of 29 lightguide bundles made of Kuraray multiclad fibers. The light loss per channel resulting from insertion of a bundle and its two connectors was measured to be about 5 dB for 8-m-long bundles. It is consistent with a clear fiber attenuation length of 10 m and a transmission efficiency of about 90% per connector joint.

The results of these measurements validate the design and construction procedure used, and it is expected that a similar and advanced procedure will be employed in fabricating clear lightguide fiber bundles for the scintillating fiber tracker as well as the central and forward preshower detectors. One slight complication is the change to v-groove connectors at the detector end of the waveguide bundles. This requires the detector end of the bundle to have a ribbon configuration (at least for a short length) and to lay in the connector, as opposed to threading individual fibers into connector holes. The fiber used for the final waveguide bundles will once again be clear, multiclad fiber from Kuraray.

Although much of the design and development work for the waveguide bundles was done at UIC, the fabrication of the bundles for the final detector has been moved to the University of Notre Dame.

VII.4.2 Lightguide bundle maker

The UIC machine shop made a lightguide bundle maker employing a motorized fiber pulling system. Figure VII-6 shows schematically the lightguide bundle maker.

The objective of the bundle maker is to allow for various bundle lengths, from 8 m to 11 m with each fiber in any one bundle having the same length. It will be used extensively for the 256-channel lightguide bundles for the scintillating fiber tracker and also used to make the 16-channel bundles for the preshower detector. One person is needed to assemble the bundles having an access to both ends at the same time. The fiber spool is placed on top of the left wheel and a tension adjustment is made to keep the feed smooth. The fiber will pass through a belt guide and a cleaner pad soaked in ethyl alcohol. A laser gauge system [10] will be used to check fiber diameter continuously during fiber pulling. A spring-loaded clamp assembly is fused to the belt. The end of the fiber is attached to the clamp and is pulled around the belt. With the maximum speed of the motor, it takes about 30 seconds for a full 11-meter pulling. The fiber will be held by friction on the belt and the spring force of the clamp. Once the fiber has made one complete turn, the motor pulling the fiber is stopped. The fiber is cut to the length with the flat face of a single-wedge blade so that the light transmission can be checked. Any fiber with significantly low light transmission (10% away from the normal fibers) will be checked and replaced if necessary. The tension on the pulley is relaxed momentarily and the fiber falls off the pulley and into split PVC pipe troughs. The operator takes one end at a time and places the ends into connector setups. Fibers will be placed into the PVC troughs. Adjustment of bundle length will be made by moving the two front wheels. The belt needs to be changed when a length adjustment is made.

The lightguide bundle maker will be installed in room 401 of Nieuwland Science Hall at Notre Dame. The total length of the device is about 5 meters and at its widest, the width is 3.5 meters. There is enough room for the computer and other electronics at the corner of the room.

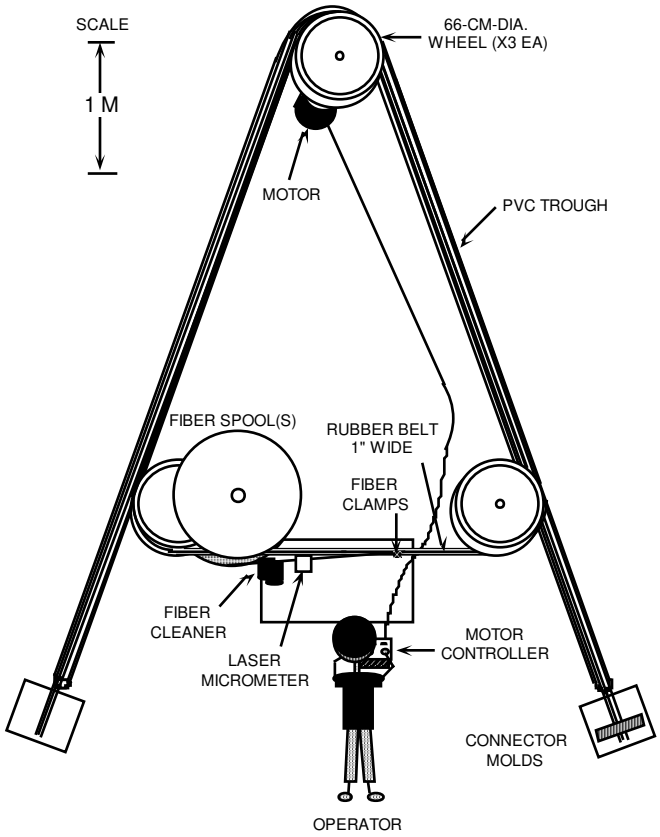

Figure VII-6 Schematic of Bundle Making Apparatus

VII.4.3 Bundle assembly procedure

The cassette end of the bundle will have the sixteen 16-channel cassette-end connectors that will mate with the two 128-channel warm-end connectors on top of the VLPC cassette cryostat. The other end of the bundle will have a 256-channel curved connector appropriate to a specific detector radius.

Sixteen-channel lightguide bundles will be made using the following steps. Using the lightguide bundle maker that is described in the previous section, 16 pieces of fiber of an appropriate length (for example, 11.1 m) are cut one by one. After grouping 16 fibers, one end of the bundle will be placed in a black plastic sleeve about 1 m long for protection and keeping light-tight. Then, the fibers' VLPC ends will be stuffed into holes of the 16-channel connector molds randomly. The 16-channel connectors will be made by casting white hard polyurethane around the fibers. After curing, the faces of the connectors will be finished using a diamond fly-cut machine at Fermilab. Sixteen such 16-channel bundles will be grouped together and assembled in a 256-channel curved

connector. A computer-controlled light source system will be used to correctly order the fibers into the curved connector. Then, Bicron BC-600 epoxy will be applied to the connector and cured overnight. The bundle assembly will be enclosed by 3/4"-diameter black PVC jacket manufactured by the Zippertubing Co [8]. The final bundle will have strain reliefs assembled on both ends. The strain relief on the cassette-end connector is designed as a cast boot of soft polyurethane, and the strain relief on the detector end has yet to be designed. The strain reliefs protect fibers from damage during handling and, along with the black PVC jacket, keep the fibers light-tight. The curved connector of the bundle will be placed in a clamp for diamond fly-cutting. After finishing the connector surface, final testing will be made for continuity and light transmission. The assembly procedure is summarized as follows:

A. Sixteen-channel fiber bundles

1. Pull the fiber on the bundle maker with on-line check by LaserMike[10].
2. Cut the fiber to the length (for example, 11.1 m).
3. Check the light transmission using a single-fiber measurement setup.
4. Repeat steps 1 to 3 to make a group of sixteen fibers.
5. Place the right side of the bundle into a 4'-long black plastic sleeve, and tie the left side (detector end) and along the fiber bundle.
6. Move the 16-channel bundle to a wall-mounted shelf.
7. Repeat steps 1 to 6 to make a group of sixteen 16-channel bundles. Dip one end of the group of 16 fibers into a silicone primer (General Electric SS4004).
8. Assemble the right-side ends into 16-channel connector molds randomly.
9. Cast the sixteen 16-channel connectors.
10. Leave the connectors overnight for curing at room temperature (option: 2 hours at 100 degree F).
11. Cast the boots on the connectors and the sleeves.
12. Leave the boots overnight for curing at room temperature (option: 2 hours at 100 degree F).
13. Number and label each 16-channel bundle by wrapping a label around the plastic sleeve.
14. Finish front faces of the 16-channel connectors by P-3, sixteen connectors at a time.
15. Put an alignment pin into one hole on each 16-channel connector.

B. 256-channel fiber bundles

16. Connect the finished face of a 16-channel connector to a testing connector that is connected to the sequencing light source.
17. Run the computer program for light sequencing.
18. Following the light, place the free ends of the fiber bundle into the correct v-grooves in a 256-channel curved connector.
19. Repeat steps 18 to 20 for sixteen 16-channel bundles until all 256 fibers have been placed into position.
20. Perform the sequence check and light transmission check before gluing.
21. Apply Bicron BC-600 epoxy to the curved connector.
22. Wait overnight for curing.
23. Put the 3/4-inch-diameter black Zippertubing jacket along the bundle.
24. Assemble a strain relief (or a boot) behind the curved connector.
25. Number and label the 256-channel bundle.
26. Repeat steps 18 to 27 to make a group (for example, ten 256-channel bundles).
27. Finish the front faces of the curved connectors by P-3.
28. Put alignment pins into the holes of the 256-channel connectors.
29. Perform the final tests of the sequencing and light transmission.

VII.4.4 Quality control and testing

A multi-channel fiber tester has been constructed with the help of the UIC electronics and machine shops. The tester utilizes computer control to flash up to 256 LEDs and read out the resultant 256 photo-transistor (photo-TR) outputs. To help in developing an automatic fiber bundle tester, a 16-channel prototype tester was made. Light sources selected are green LED bargraph units, with which we studied light output as a function of applied voltage and as a function of time. A photo-TR was chosen as light detector because it can be used in a simple DC mode without an amplifier. The program in the prototype testing was written in Quick BASIC. The multi-channel tester includes a 16-channel analog-to-digital converter (ADC) and analog multiplexers (AMUX) by National Instruments. It will test a lightguide bundle of up to 256 channels. The setup is schematically shown in Fig. VII-7.

In the LED box, the decoder can turn on the LEDs one by one in sequence or all at once. It takes about 0.2 second to turn on 256 channels one by one. The light detection is made by the photo-TR box. With the four analog multiplexers, AMUX-64, and data acquisition board, AT-MIO-16E-10, from National Instruments, the Pentium PC reads all 256 channels in two seconds.

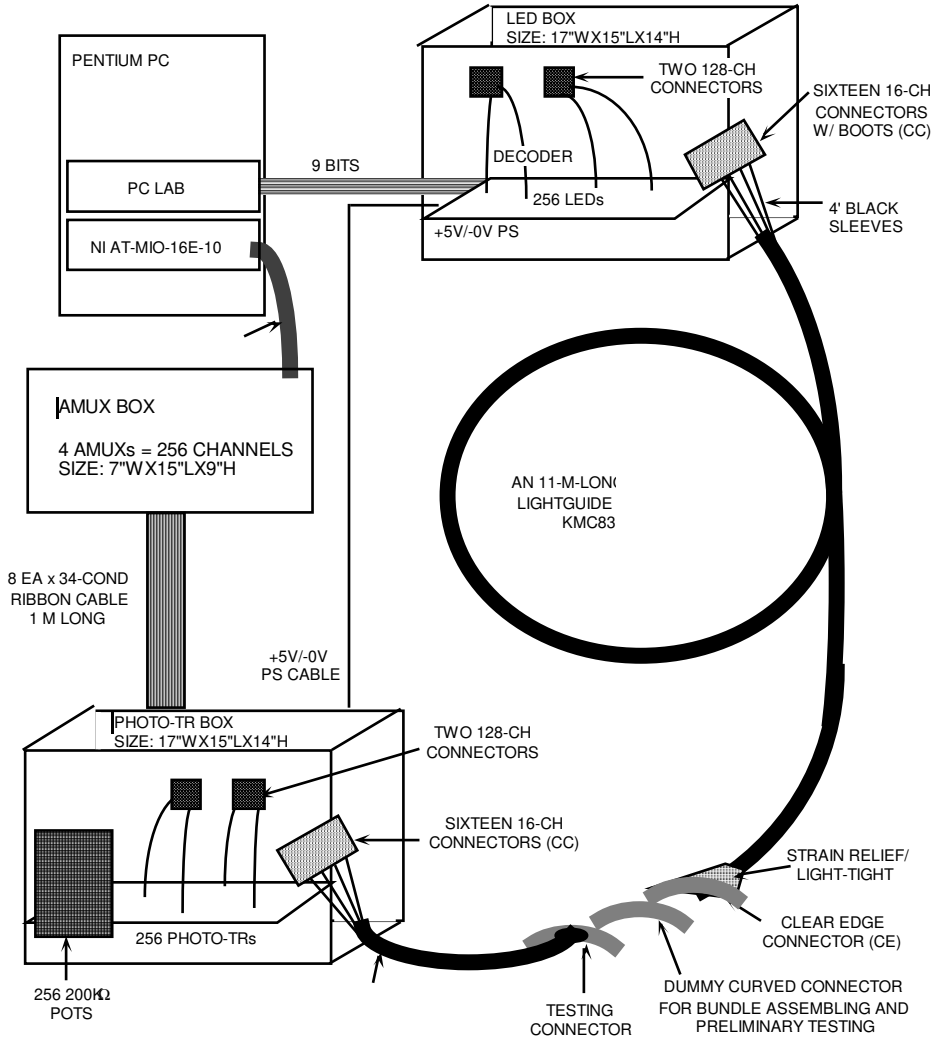

Figure VII-7 Schematic of Bundle Testing Apparatus

Quality control is important in making reliable bundles with a minimum of bad channels. A preliminary check before gluing is essential to screen bad channels and any human errors. It includes a sequence check to confirm the correct continuity and a measurement of light transmission to detect a bad fiber. We need a simple fiber end finishing technique that is reproducible enough to allow screening. During our preliminary testing we optimized the fiber end finish by testing the cuts made using a few different knife blades. We found that the flat face of a single-wedge blade gives a better fiber-end surface, resulting in more light transmission. Using 100 pieces of 36-cm-

long0.965-mm-diameter Kuraray multiclad S-type clear fiber, we measured a light transmission of 77%±4% when we cut both ends of the fibers using the single-wedge blade as compared to 100% for fibers with both ends cut using a single-fiber diamond fly-cut tool [9]. A normal razor blade of the double-wedge type resulted in only 33%±2% transmission.

The final testing of each bundle will be made after gluing and surface finishing with the P-3 diamond fly-cut machine. The continuity is checked again for confirmation and bookkeeping. The light transmission through all channels will be measured and the channel-to-channel variation will be determined. We anticipate less than ±10% variation.

An absolute comparison between bundles will be made by keeping a few control bundles and measuring for comparison with the bundles being produced. To control the quality of the bundles, attenuation lengths of different batches of fibers will be monitored by making one set of fibers with lengths of 1 m, 3 m, 5 m, 10 m, 15 m, and 20 m for the incoming fiber spools with the frequency of about one set of fibers in four months. They will be used to estimate the attenuation length of the fibers and also to understand the fiber-to-fiber variation. By measuring the sets of fibers once in every four months, any possible long-term fiber aging will also be followed.

A computer program will be written for production control and bookkeeping. The program is required to make and update inventory listings of the incoming fiber spools, various connectors, produced lightguide bundles, and their test results. The same program will record the transmission and continuity results and do the bookkeeping on all the bundles for the various stages of the assembly. Each produced bundle will have tags attached summarizing its history and test results.

VII.4.5 Connection and Routing of Waveguide Fibers

The installation of the clear waveguide fibers involves careful mapping and routing of the fiber bundles. The VLPCs are located 6 meters below the center of the central cryostat. The waveguide bundles must be routed from the tracker to the VLPCs through the relatively small gap between the central and endcap cryostats, as illustrated in Fig. VII-8. A significant fraction of this gap is also occupied by the forward preshower detector, which has its own waveguide fibers which must be routed to VLPCs.

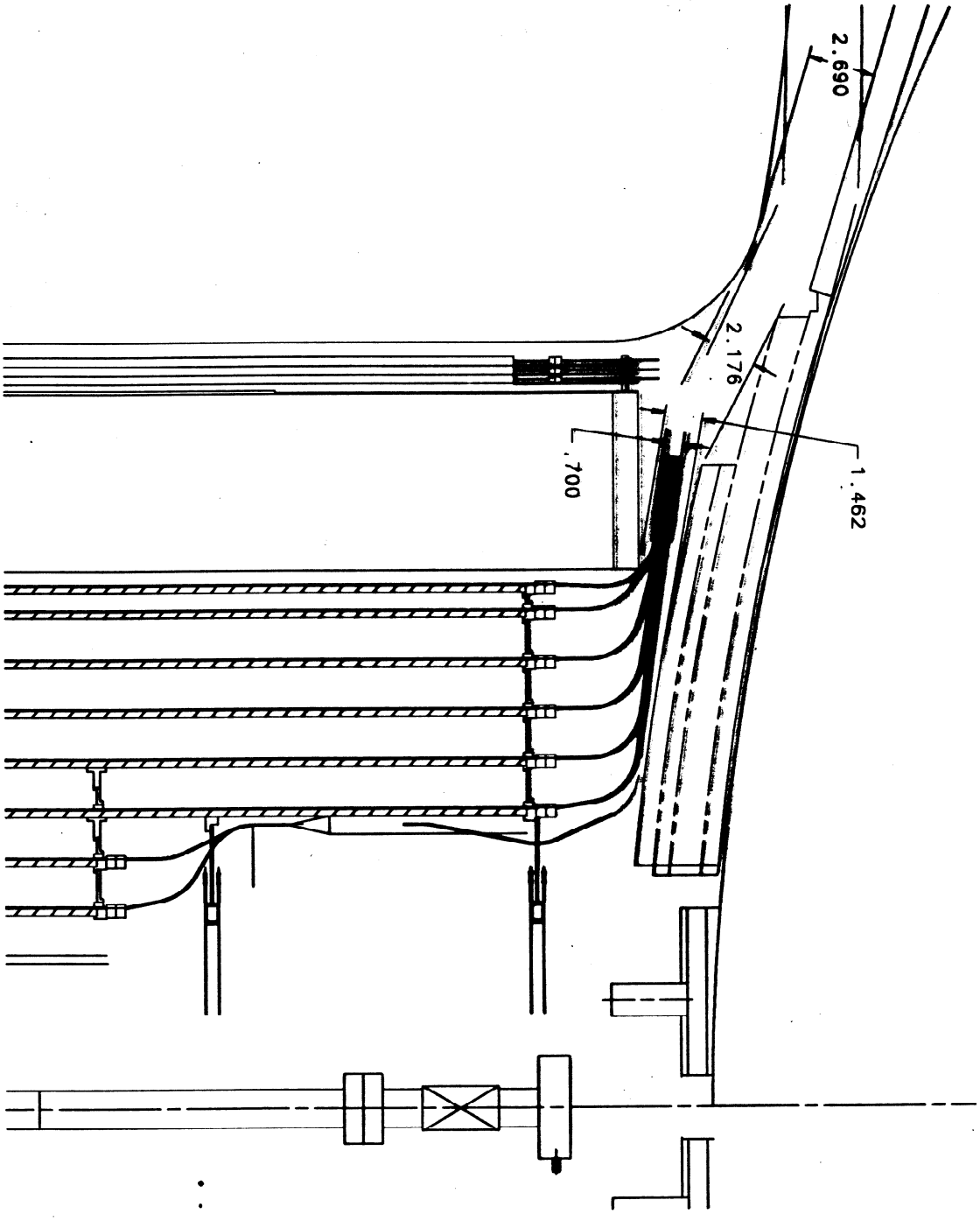
2.690
2.176
1.462
,700

Figure VII-8 Cross section view of the DØ upgrade tracking system illustrating the routing of the clear waveguide fiber bundles.

The waveguide bundles are connected to the fiber tracker using curved connectors which follow the circumference of each individual layer of the tracker in units of 256 fibers. The natural inclination of the waveguide bundles, because of the curvature of the connectors, is to curl up immediately into cylinders. The minimum gap through which the fibers must pass, defined by the edge of the solenoid magnet and the forward preshower, is 1.5 inches. We have recently begun a detailed layout of the waveguide fibers as they come off of the tracker to understand if this gap is sufficient. If it is not, we will have to defer transition to cylindrical bundles and bring the waveguide fibers off of the tracker as flat ribbons until they clear the forward preshower.

Once the waveguide fibers have cleared the forward preshower, they must be arranged on the face of the central cryostat in such a way as to distribute the slack which will systematically develop as one moves from the top of the tracker to the bottom. This will allow for the bundles to arrive at the electronics platform with their far ends approximately aligned. The waveguide bundles will make their way to the electronics platform through notches which have been cut out of the steel beams which support the detector.

The far end of the waveguide bundles which carry light from the stereo fibers will terminate in two rectangular connectors of 128 fibers which will connect to 128-fiber warm-end optical connectors on the VLPC cassettes. The situation is somewhat more complex for the waveguide bundles which correspond to the axial fiber layers since they must participate in the trigger. For triggering purposes, the tracker is segmented into 80 sectors in the ϕ angle. Fibers from each axial layer of the tracker which lie in the same phi window are grouped together. Included in each trigger sector are the fibers from the central preshower detector which lie in the appropriate ϕ window. More specifically, the fibers within a trigger sector are grouped by layers according to the scheme A+H, B+G, C+F, and D+E, where the letters A-H denote the eight support cylinders ordered from innermost to outermost cylinder. Each of these groupings results in a total of 120 fibers. These are each combined with sets of 8 fibers from the central preshower for a total of 128 fibers which are routed to a single 128-fiber warm-end optical connector on a VLPC cassette.

The 80 trigger sectors do not, as a rule, align themselves along connector boundaries. It is not uncommon for the fibers from a particular tracker layer which lie in a single trigger sector to span two waveguide bundles. This is why the waveguide

bundles described above terminate in sixteen individual 16-channel connectors at the VLPC end. Another way to handle this mismatch between the physical detector layout and the trigger topology would be to add an interface which allows fibers from different waveguide bundles to be grouped and routed to the appropriate cassette channels. Two such interfaces are being investigated; a mixing box and a patch panel.

The mixing box solution consists of a box into which waveguide bundle connectors, each containing 256 fibers, terminate. On the other side of the box, fibers grouped in units of 128 emerge and run to the VLPC cassettes. Inside of the box is a network of fibers which map the input fibers to the appropriate output in order to satisfy the trigger geometry.

The patch panel solution makes use of the fact that the waveguide bundles, when grouped in units of 8, can be arranged into combinations which correspond to the trigger sector geometry (8 is the largest number for which this works, unfortunately). In this scheme, each of the waveguide bundles would terminate onto 32 8-fiber connectors. Sixteen of these 8-fiber connectors would attach to a 128-fiber block connector in combinations appropriate for the trigger scheme. The patch panel would consist of an array of these block connectors. The output from each of the block connectors would consist of 120 fibers from two tracker layers (A+H, B+G, etc.) which lie within the same trigger sector, plus 8 fibers from the central preshower detector. These fibers would run to a 128-channel warm-end optical connector.

In both of the interface schemes described above, a trade-off is made between easier installation (and perhaps fabrication) of the clear waveguide bundles versus some loss of scintillation light due to the extra one or two optical connections required. Another complication is to find sufficient space under the detector to place either the mixing boxes or patch panels.

VII.5 Environment Control

Connectors, barrel end rings and annular connecting disks seal the fiber volume, so that a small flow of nitrogen (depending on leak rate, which has still to be determined) will be sufficient to exclude ambient air (oxygen, moisture) from the atmosphere surrounding the scintillating fibers. This enclosure should also be sufficiently light tight. The wave guides are contained in protective and light tight sheathing. Light tightening of the fiber routing area above the VLPC cassettes will probably rely on a combination of individual wave guide shielding and light tight enclosure of the volume above the cassettes. The cooling of the cassette electronics boards should not stand in the way of

light tightening, since the forced air flow to the cassettes is by ductwork, and it might be preferable to use ductwork also for the warm exhaust air.

VII.6 References

[1] "Scintillating fibers position measurement in curved ribbons using an x-ray source", G. Guttierez, DØ Note 3380

[2] DØ Note 1601

[3] "Fabrication and testing of clear lightguide fiber bundles for the D0 prototype fiber tracker cosmic-ray test", S. Margulies and M. Chung, in Scintillating Fiber Technology and Applications II, ed. E.J. Fenyves, Proc. SPIE **2281**, pp. 26-34, 1994.

[4] Kuraray International Corporation, 200 Park Avenue, New York, NY 10166.

[5] "Aging studies on stressed and unstressed scintillating, wave-shifting, and clear fibers", M. Chung and S. Margulies, in Photoelectronic Detectors, Cameras, and Systems, eds. C.B. Johnson and E.J. Fenyves, Proc. SPIE **2551**, pp. 2-9, 1995.

[6] Bicron Corporation, 12345 Kinsman Road, Newbury, OH 44065.

[7] "Test of epoxies for attaching Kuraray multiclad fibers to Delrin", M. Born, M. Chung, and S. Margulies, DØ Note **1776**, 29 June 1993.

[8] The Zippertubing Co., 13000 S. Broadway, Los Angeles, CA 90061.

[9] The diamond fly-cut tool for connectors was designed and made at the Physics Department, Fermilab, Batavia, IL 60510. The single-fiber diamond fly-cut tool was made by Avtech, Advanced Technology and Design Inc., 625 Schneider Drive, South Elgin, IL 60177.

[10] LaserMike and FiberMike are products of LaserMike Inc., 8001 Technology Blvd., Dayton, OH 45424.

Chapter VIII. Monitoring and Calibration

VIII.1 Temperature Control and Monitoring

VIII.1.1 Detector

Since the fiber detector itself contains no heat generating components, the main possible sources (and sinks) of heat are the Silicon Tracker, and the superconducting coil.

Calculations for the coil [1] show that even in the case of a quench the change in temperature in the outer CFT cylinder would be negligible. A catastrophic failure of the magnet's vacuum jacket could cause a significant drop in the temperature of the outer fiber cylinder, but the system has been designed to ensure that the risk of such a failure is extremely small.

A series of interlocks will ensure that the power to the silicon tracker is shut off in the event of any problem with the silicon cooling system. This will eliminate the risk of heating up the innermost CFT cylinder. When the silicon cooling system is operating, however, the outer region of the silicon detector will be well below room temperature. To keep the inner CFT cylinder from cooling down, dry gas will flow in the gap between the outside of the silicon tracker and the inner fiber cylinder [2].

VIII.1.2 VLPC Temperature Control and Monitoring

The temperature control system for the operation and monitoring of the VLPC readout system is discussed in detail in the VLPC cassette TDR [3]**.** The following is a brief overview of the system and its key components.

The 1024 channel VLPC cassettes are segmented into eight modules of 128 channels each. Each module has a heater/sensor card (HSC) containing one temperature sensor and 2 heaters. The card is mounted on the bottom of the isotherm which keeps all the VLPCs at a common operating temperature. Since all eight modules within a cassette are thermally coupled, it is expected that a single temperature sensor will be used to control all the heaters within the cassette.

The temperature sensor is a standard 1/4 Watt carbon film resistor with a nominal resistance of 100 Ω at room temperature. The resistance is inversely proportional to temperature and increases to about 500 Ω at 6.5 K, with a sensitivity on the order of 100

Ω per Kelvin. The resistors are mounted on the HSC and then calibrated at Fermilab. The precision of the calibration is better than 1 mK = 0.1 Ω at a temperature of 6.5 K.

The heater resistors are standard metal film resistors of 500 Ω nominal value, 1/8 Watt, which exhibit a resistance of 500 Ω also in the operating temperature range.

Several industrial controllers have been successfully tested for compliance with electrical noise and temperature stability requirements. It is intended to integrate the temperature control and monitoring of the VLPC system into the overall DØ cryogenics control using FIX-DMACS.

VIII.2 Calibration System

The calibration system for the fiber tracking detector is being designed to perform several functions. The system will enable the gains of each fiber-VLPC channel to be determined, allow monitoring of the stability of the VLPC readout over time, provide a measure of each scintillating fiber's attenuation length as the experiment progresses, and the calibration system will serve as a useful debugging tool during the commissioning of the tracker.

In order to determine the gains of the VLPC channels, the calibration system must be capable of illuminating each VLPC pixel with a small amount of light, typically a few photons. One way to do this is by exciting the scintillating fibers with a radioactive source, but this method has been judged to be difficult and impractical. A second method is to introduce visible light into the fibers, which in turn "pipe" the light down to the VLPCs. This method was successfully employed in the system test described in Section VI. In the test, red LEDs were used to inject light into each scintillating fiber via short (2 meter) clear waveguide fibers mated to the scintillating fibers at the non-readout end of the tracker. Each of the 3,072 LEDs were under computer control and were individually selectable. A schematic view of a single fiber channel with its calibration LED is shown in Fig. VIII-1. A typical VLPC calibration spectrum is shown in Fig. VIII-2. More details of this calibration system can be found in reference [4].

Given the success of the calibration method used in the system test, a similar scheme was initially envisaged for the fiber tracker. However, the limited space at the ends of the tracking cylinders make it very difficult to introduce light into the ends of the scintillating fibers. A new method has been devised which uses the availability of new, fast blue LEDs to introduce light through the cladding walls and into the active core of the fiber. The idea, shown schematically in Fig. VIII-3, takes advantage of the fact that

the 3HF dye in the fibers have a small, but finite absorption in the blue wavelength range (~450 nm). When blue light is incident upon several layers of scintillating fiber, as shown in the figure, a small amount is absorbed in the top layer and excites the 3HF dye, producing scintillation photons which are detected by the VLPC. However, since the absorption in this wavelength is small, most of the light travels on into subsequent layers of fiber. In this way the light source can excite fibers several layers deep, as shown in the figure.

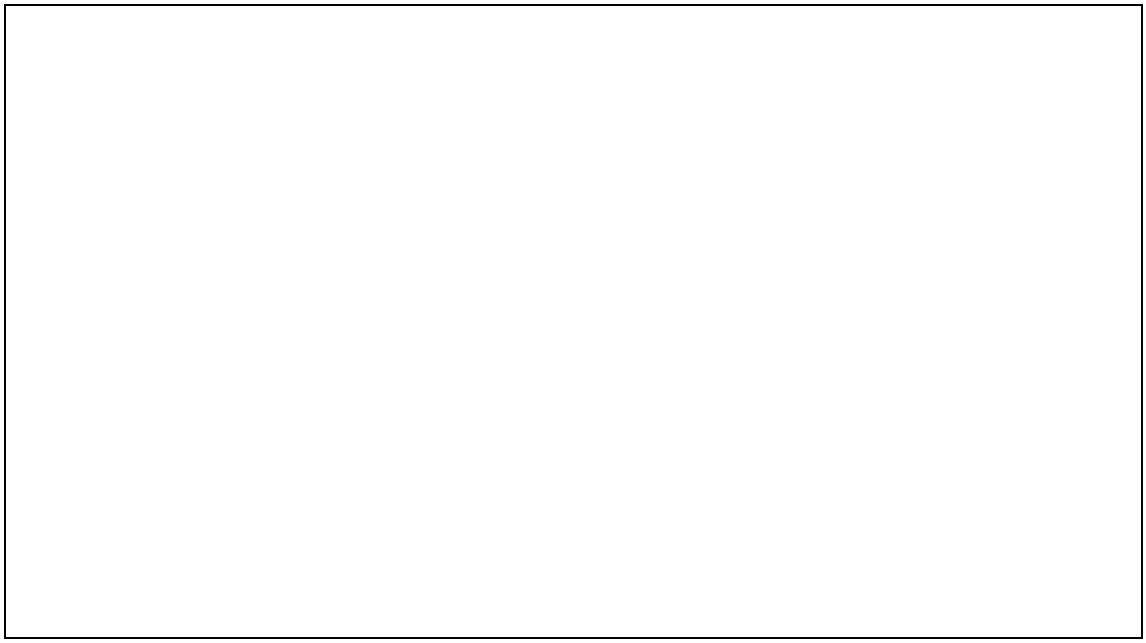

Figure VIII-1 LED Schematic view of a single channel in the system test. The calibration is indicated in the upper left corner of the figure.

Figure VIII-2 Typical calibration spectrum of a VLPC channel in the system test. The gain is defined as the difference, in ADC counts, of the means of the pedestal and first photoelectron peaks.

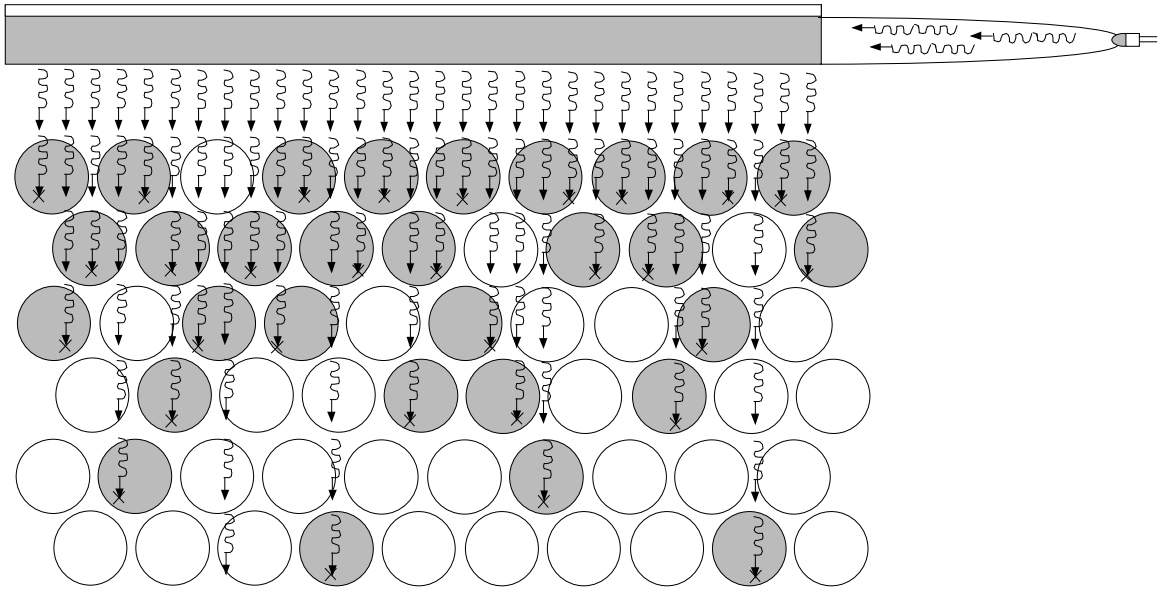

Figure VIII-3 Blue LED light calibration scheme

Initial tests of this method were performed at Notre Dame. In these tests, a small number of LEDs (usually two) were inserted into a lucite block covered with a thin

diffusing material. The block was placed above a stack of three doublet layers of scintillating fiber. Each fiber layer was 96 fibers wide, but since the readout system available contained only 32 channels of VLPC, very 12th fiber was read out from four of the six fiber layers for a given test. Data were taken for a variety of LED types [5], and at different locations in the lucite block. The results firmly established proof-of-principle of the technique. As few as two LEDs easily provided enough light to excite fibers in all six layers across the entire 96-fiber ribbon width, and the spectra obtained were adequate for determining the VLPC gain.

In order to apply the blue LED calibration method to the fiber tracker, a means of distributing the light over of the cylindrical geometry of the tracker is necessary. A promising solution to this problem is the optical flat panel, illustrated in Fig. VIII-4. These can be fabricated in several ways, but the basic design consists of a single, thin ribbon of small (typically 500 μm diameter) clear fibers which have been degraded in a certain region so that light is emitted through their cladding wall. At one end of the ribbon, the fibers are bundled together, potted and finished to allow mating with an LED or external optical fiber. Thus external light entering the flat panel through the ends of the fibers is distributed uniformly across a flat, predetermined area. These devices are commonly used in the fabrication of flat panel displays for computers. The panels are extremely light, flexible, and conform easily to a cylindrical surface.

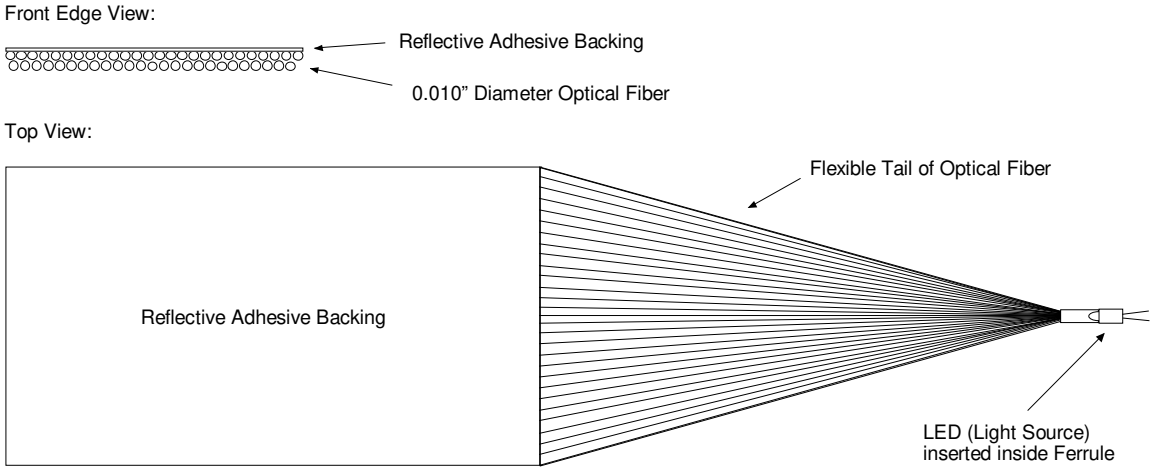

Figure VIII-4 Schematic view of an optical flat panel

Test samples have been obtained from two manufacturers of these panels [6] and measurements have been performed at Notre Dame to determine the feasibility of using such devices for the calibration system. The test apparatus was essentially identical to that described above, except that the lucite block with embedded LEDs was replaced with a single optical panel illuminated with a blue LED. The results were very encouraging. Figure VIII-5 shows spectra from the bottom layer of the 6-layer deep fiber ribbon. The four plots correspond to four fibers spanning the width of the 96-fiber wide ribbon. The spectra clearly show that: 1) sufficient light penetrates the six fiber layers to provide a calibration of even the bottom layer, and 2) the illumination provided by a flat panel with a single LED is very uniform over a ribbon width of order 100 fibers.

For the final calibration design, two methods of illuminating the optical panels are under study. In the first method, each panel would have a blue LED coupled directly to its bundle of fibers, at the detector. Each LED, in turn, would be mounted on a small printed circuit board which would provide the necessary electronics to drive the LED. This board is under design at Notre Dame. In the second method, the blue LEDs would be located external to the tracker, and the LED light would be fed to the optical panels via a fiber waveguide. Test prototypes of both methods will be constructed at Notre Dame and compared before the final design decision is taken.

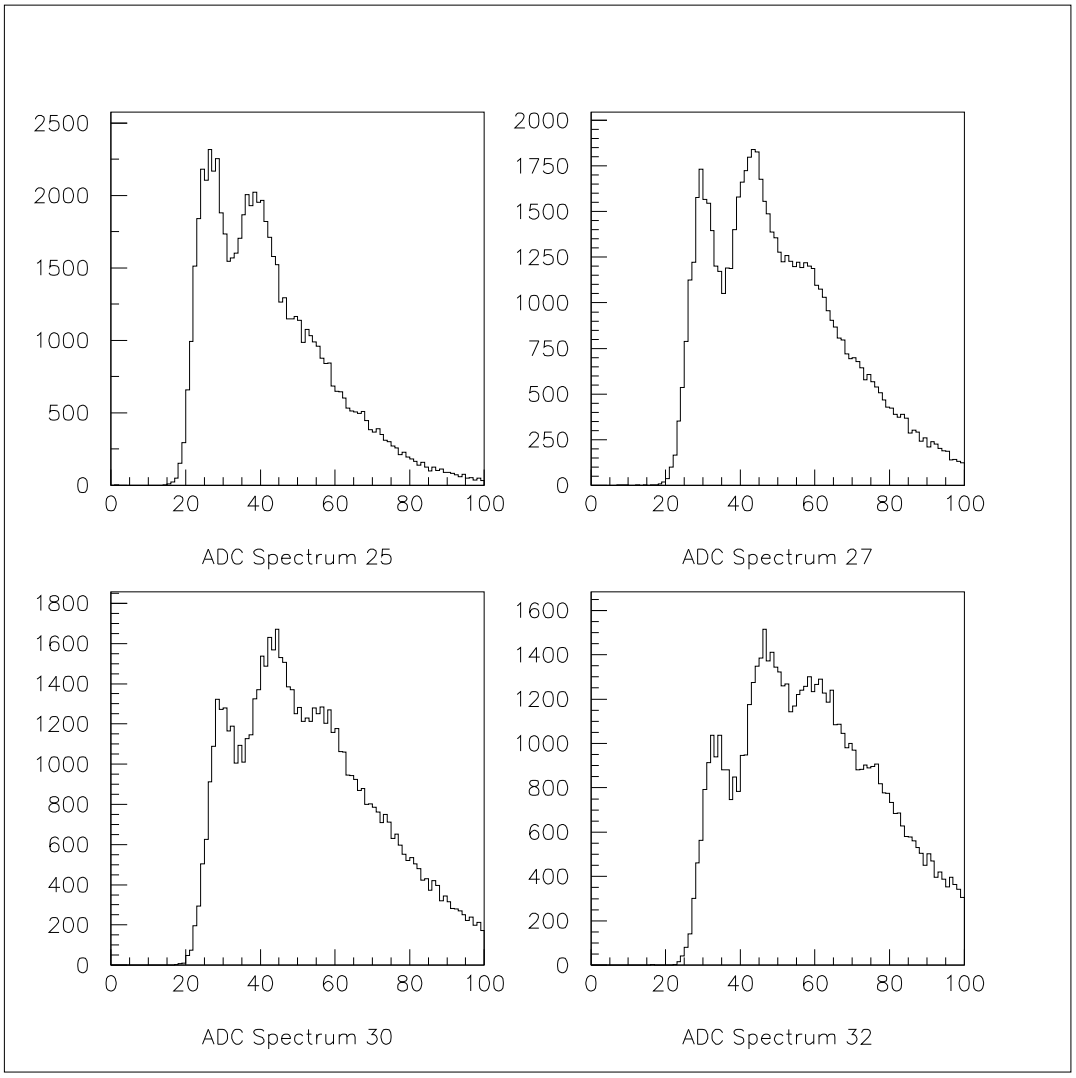

Figure VIII-5 Spectra from four fibers at the bottom of a six-layer deep fiber ribbon, illuminated from above by an optical flat panel with a blue LED.

The mounting scheme for the final calibration system is shown schematically in Fig. VIII-6. The flat optical panels are mounted around every scintillating fiber cylinder in bands near each end of the cylinder. The bands will be plastic extrusions cut to length to fit each cylinder. Placing two bands on each cylinder provides an extra margin of safety against the failure of an individual optical element. Also, by comparing the total light seen at both ends of the tracker, potential changes in the quality of the scintillating fiber can be monitored over time.

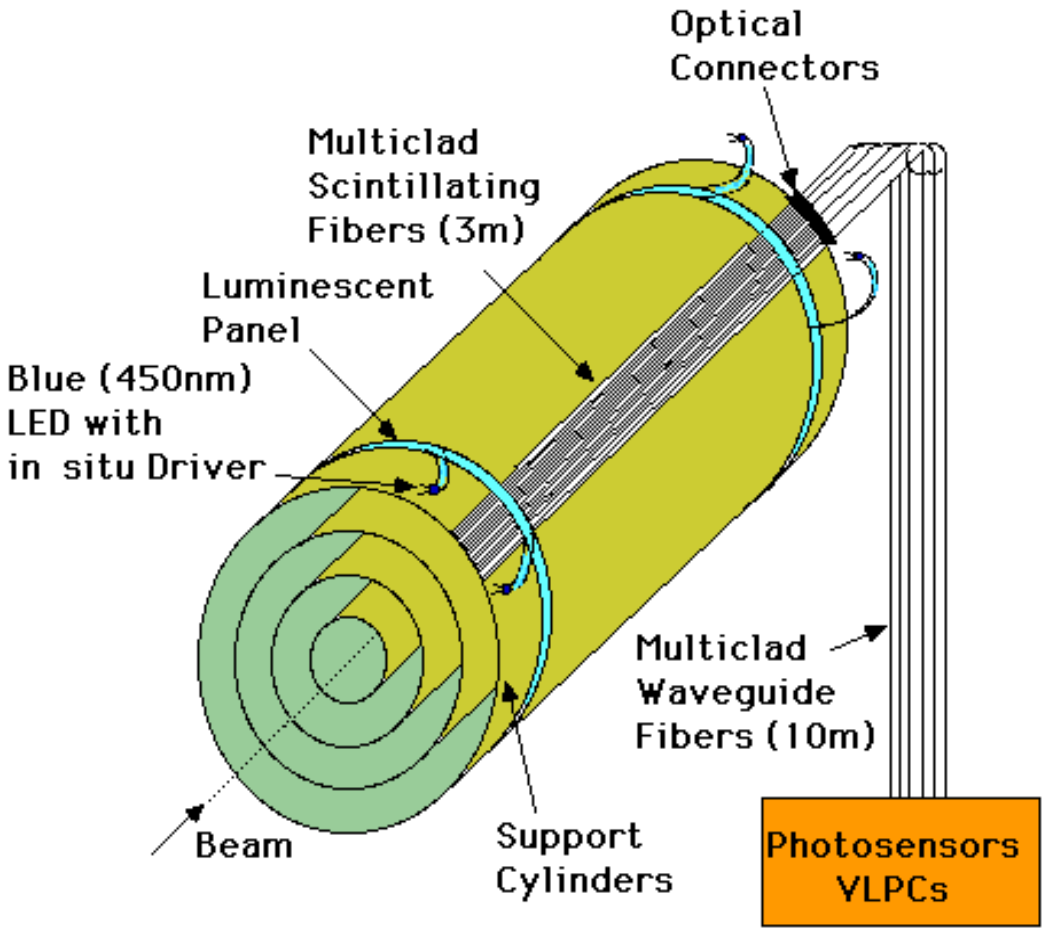

Figure VIII-6 Illustration of the mounting scheme of flat optical panels for the CFT calibration system

VIII.5 References

[1] G. Fisk & K. Krempetz (private communication)

[2] B. Squires (private communication)

[3] "DØ Fiber Tracker 1024 Channel VLPC Cassette Technical Design Report and Specification"

[4] B. Baumbaugh et al., IEEE Trans. Nucl. Sci., Vol. 42, No. 4, 1995, 383-386

[5] Ledtronics Inc., 4009 Pacific Coast Highway, Torrance, CA 90505;
Nichia America Corp., 3775 Hempland Rd., Mountville, PA 17554

[6] Lumitex Inc., 8443 Dow Circle, Strongsville, OH 44136;
Poly-Optical Products Inc., 17475 Gillette Ave., Irvine, CA 92714